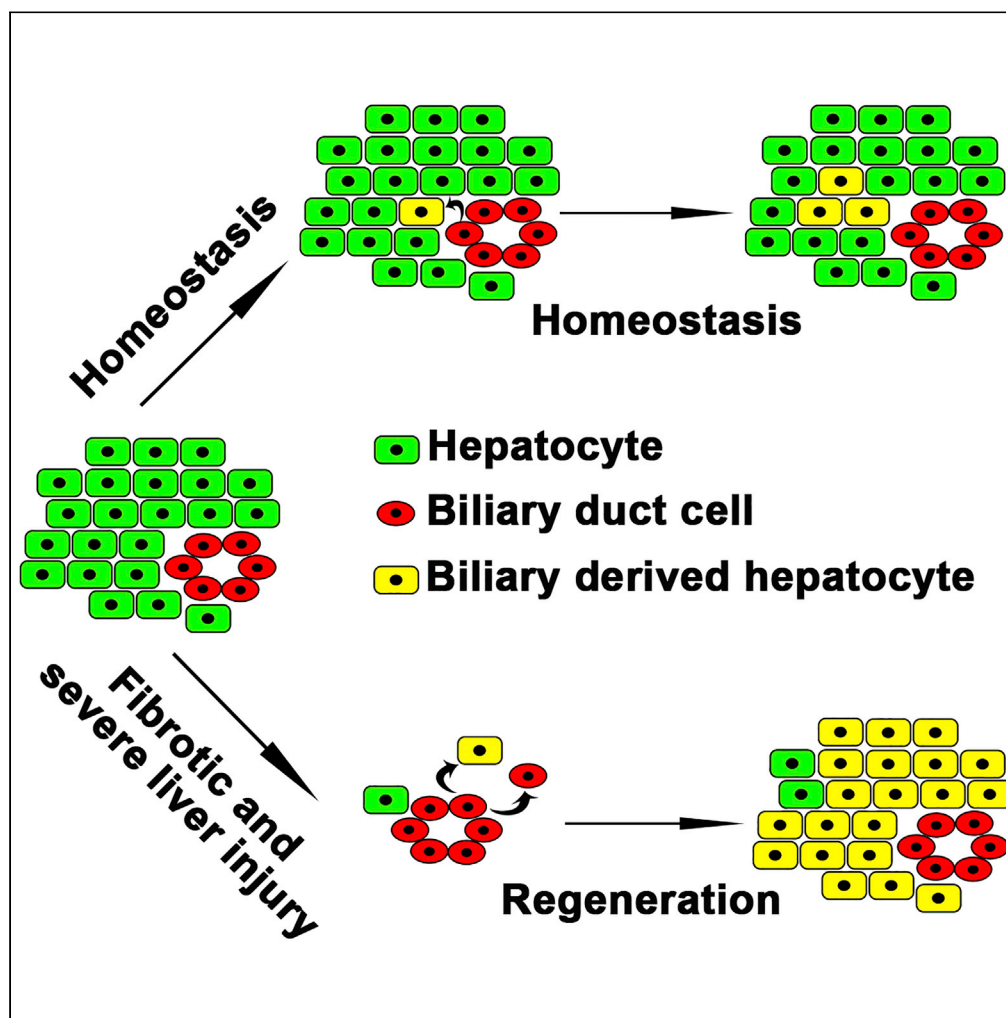**Article**

Contributions of biliary epithelial cells to hepatocyte homeostasis and regeneration in zebrafish

Wenfeng Zhang,
Jingying Chen, Rui
Ni, Qifen Yang,
Lingfei Luo,
Jianbo He

lluo@swu.edu.cn (L.L.)
hejianbo@swu.edu.cn (J.H.)

HIGHLIGHTS

Developed sensitivity
system to trace BECs
derived hepatocytes in
liver homeostasis

BECs convert to
hepatocytes in liver
homeostasis but are
individually
heterogeneous

BECs are the primary
regeneration sources in
the extreme injury of the
fibrotic liver

BECs fail to contribute to
new hepatocytes after
partial hepatectomy

CellPress
OPEN ACCESS

Article

Contributions of biliary epithelial cells to hepatocyte homeostasis and regeneration in zebrafish

Wenfeng Zhang,[1] Jingying Chen,[1,2] Rui Ni,[1] Qifen Yang,[1] Lingfei Luo,[1,*] and Jianbo He[1,3,*]

SUMMARY

Whether transdifferentiation of the biliary epithelial cells (BECs) to hepatocytes occurs under physiological conditions and contributes to liver homeostasis remains under long-term debate. Similar questions have been raised under pathological circumstances if a fibrotic liver is suffered from severe injuries. To address these questions in zebrafish, we established a sensitive lineage tracing system specific for the detection of BEC-derived hepatocytes. The BEC-to-hepatocyte transdifferentiation occurred and became minor contributors to hepatocyte homeostasis in a portion of adult individuals. The BEC-derived hepatocytes distributed in clusters in the liver. When a fibrotic liver underwent extreme hepatocyte damages, BEC-to-hepatocyte transdifferentiation acted as the major origin of regenerating hepatocytes. In contrast, partial hepatectomy failed to induce the BEC-to-hepatocyte conversion. In conclusion, based on a sensitive lineage tracing system, our results suggest that BECs are able to transdifferentiate into hepatocytes and contribute to both physiological hepatocyte homeostasis and pathological regeneration.

INTRODUCTION

Proper control of organ volume and cell number is pivotal in the development, homeostasis, and regeneration of organs. The hepatocytes continuously proliferate to promote liver growth during development. The cell number in a liver increases by about 30–100 folds from embryonic day 14.5 to adult in mice (Rollins et al., 2010) and 900 folds from 5 days post-fertilization (dpf) to 1.5 years in zebrafish (Gao et al., 2018). The liver maintains physiological homeostasis and pathological regeneration either via the proliferation of hepatocytes and biliary epithelial cells (BECs) or via differentiation/transdifferentiation of progenitor cells or other cell types (Gadd et al., 2020; Ko et al., 2020; Miyajima et al., 2014; Stanger, 2015). Different cell origins have been identified to contribute to liver regeneration in different liver injury models (Gadd et al., 2020; Ko et al., 2020; Li et al., 2020). The cell origin of hepatocyte homeostasis and regeneration is a fundamental topic in hepatology.

The identity of cell origins for normal liver homeostasis and regeneration remains under debate. During development, both hepatocytes and BECs originate from hepatoblasts. In the functional liver, if the self-renewal of remaining hepatocytes is inhibited after severe liver injury, liver progenitor cells (LPCs) appear and give rise to both hepatocytes and cholangiocytes (Duncan et al., 2009). During chronic injuries in rodents, the BECs are activated to form oval cells, also called ductular reactions, and then differentiated into hepatocytes (Evarts et al., 1987; Sato et al., 2019; Wang et al., 2003; Yovchev et al., 2008). Most studies indicate the LPCs are mainly derived from BECs (Furuyama et al., 2011; Lu et al., 2015; Raven et al., 2017; Rodrigo-Torres et al., 2014; Tarlow et al., 2014a). However, only 1.86% of total hepatocytes after liver injury are derived from the Hnf1β[+] BECs (Rodrigo-Torres et al., 2014). LPCs in bile ducts have also been reported to contribute to hepatocytes during liver homeostasis and after 2/3 partial hepatectomy (PH) (Furuyama et al., 2011). However, other reports demonstrate that hepatocytes self-renew as a paradigm for liver regeneration and exclude BECs or LPCs as cellular origins of hepatocyte regeneration, and Sox9^{+} BECs have no contribution during liver homeostasis (Carpentier et al., 2011; Malato et al., 2011). Furthermore, the Sox9^{+} ductal progenitor cells give rise to clonal oval cells and bipotential organoids but rarely produce hepatocytes (Tarlow et al., 2014a).

[1]Institute of Developmental Biology and Regenerative Medicine, Southwest University, 2 Tiansheng Road, Beibei, 400715 Chongqing, China

[2]University of Chinese Academy of Sciences (Chongqing), Chongqing Institute of Green and Intelligent Technology, Chinese Academy of Sciences, Beibei, 400714 Chongqing, China

[3]Lead contact

*Correspondence: lluo@swu.edu.cn (L.L.), hejianbo@swu.edu.cn (J.H.)

https://doi.org/10.1016/j.isci.2021.102142

Recent findings have proposed that the LPCs are derived from mature hepatocytes (Chen et al., 2013; Tarlow et al., 2014b). Although LPCs play essential roles during the toxin-induced liver regeneration (Fausto and Campbell, 2003; Huch et al., 2013; Zaret and Grompe, 2008), the hepatocytes also show plasticity (Chen et al., 2013; Lin et al., 2018; Michalopoulos et al., 2005; Schaub et al., 2014; Tanimizu et al., 2014; Tarlow et al., 2014b; Wang et al., 2015; Yanger et al., 2013). Hepatocyte self-renewal has been believed to exclusively contribute to liver homeostasis (Gao et al., 2018; Yanger et al., 2014). Multiple lineage-tracing studies in mice have shown that during chronic and acute injuries, the regenerated hepatocytes are exclusively derived from pre-existing hepatocytes (Schaub et al., 2014; Yanger et al., 2014). However, recent studies demonstrated that the BECs become major cell origins of hepatocyte regeneration after extreme hepatocyte loss in zebrafish (Choi et al., 2014, 2017; He et al., 2014; Ko et al., 2016, 2019; Russell et al., 2019; So et al., 2020) or blockade of hepatocyte proliferation in mice (Deng et al., 2018; Ko et al., 2016; Lu et al., 2015; Manco et al., 2019; Raven et al., 2017; Russell et al., 2019). Therefore, the roles of BECs in hepatocyte homeostasis and regeneration remain for further investigation.

Extensive studies have been carried out to explore the origins of newly formed hepatocytes responsible for liver regeneration after PH. After 2/3 PH, the residual hepatocytes and other liver cells rapidly grow and proliferate to accomplish the regeneration within a week (Brues and Marble, 1937; Michalopoulos, 2007; Miyaoka et al., 2012). After 30% PH, liver regeneration mainly depends on hepatocyte growth, not proliferation (Miyaoka et al., 2012). After surgical liver resection, the tritiated thymidine assay suggests that the new hepatocytes derive from the periportal area and migrate progressively toward the central vein, and this "streaming liver" model has recently been confirmed in humans (Fellous et al., 2009). However, other groups have used mosaic expression of lacZ and retroviral infection experiments to demonstrate that streaming does not occur in the quiescent liver or following PH (Bralet et al., 1994; Kennedy et al., 1995). Then, the identity of cell origins for liver regeneration after PH remains to be reconciled.

In this study, we develop a sensitive system in zebrafish to delineate contributions of BECs in liver homeostasis and regeneration using BEC-to-hepatocyte-specific lineage tracing. We find that the conversion of BECs to hepatocytes occurs in liver homeostasis. BECs do not contribute to hepatocyte regeneration after PH. But after extreme hepatocyte loss in the fibrotic liver, BECs become the primary cell sources for regeneration. These data demonstrate that BECs do contribute to form hepatocytes in physiological liver homeostasis and pathological liver regeneration after extreme injury in zebrafish.

RESULTS

Establishment of the zebrafish lineage tracing system specific for the detection of BEC-to-hepatocyte conversion

To better trace the fate of BECs in zebrafish, we constructed the transgenic line *Tg(tp1:CreERT²)*, in which the expression of CreER is under the control of a Notch-responsive element *Tp1* that is transcriptionally active in the BECs (Wang et al., 2011). By crossing this line with the *Tg(β-actin:loxP-DsRed-loxP-GFP)^{s928}* reporter line (Liu et al., 2010), Cre/loxP-mediated recombination will be able to remove the *loxP*-flanked *DsRed-Stop* cassette, leading to expression of green fluorescent proteins (GFP) to label cells. To check the possible leakiness of the *tp1*-driving CreER and the labeling efficiency of BECs, we treated the double transgenic line *Tg(tp1:CreERT²; β-actin:loxP-DsRed-loxP-GFP)* with tamoxifen (4OHT) from 5 dpf to 7 dpf and collected the larvae three days later (Figures 1A and S1A). Immunostaining for GFP and 2F11, a marker of BECs in homeostasis and progenitors in liver regeneration (He et al., 2019; Zhang et al., 2014), showed that dimethylsulfoxide (DMSO) treatment did not induce any GFP expression, whereas 4OHT treatment led to expression of GFP in 83.2% of the 2F11-positive cholangiocytes (Figure 1B). To further validate that all the GFP cells in the liver are BECs, we did immunostaining of GFP with 2F11 and Alcam (a marker of zebrafish BECs (Sakaguchi et al., 2008)) and found that all the GFP-positive cells were 2F11 positive (Figure S1B) and Alcam positive (Figure S1C) after 4OHT treatment. These data exclude leakiness of the *tp1*-driving CreER and indicate high labeling efficiency of BEC-derived cells.

We then established the *Tg(tp1:CreERT²; lfabp:loxP-STOP-loxP-DsRed; lfabp:Dendra2-NTR)* lineage tracing system specific for the detection of BEC-to-hepatocyte conversion, in which the *liver fatty acid-binding protein 10a* (*lfabp*) promoter was applied to label hepatocytes (He et al., 2014; Venkatachalam et al., 2009). Only hepatocytes derived from BECs will become positive for DsRed in this system. DsRed⁺ hepatocyte was not observed after five days after 4OHT treatment (Figure 1C), indicating that 4OHT itself did not induce BEC-to-hepatocyte conversion. Furthermore, hematoxylin-eosin staining (H&E) showed
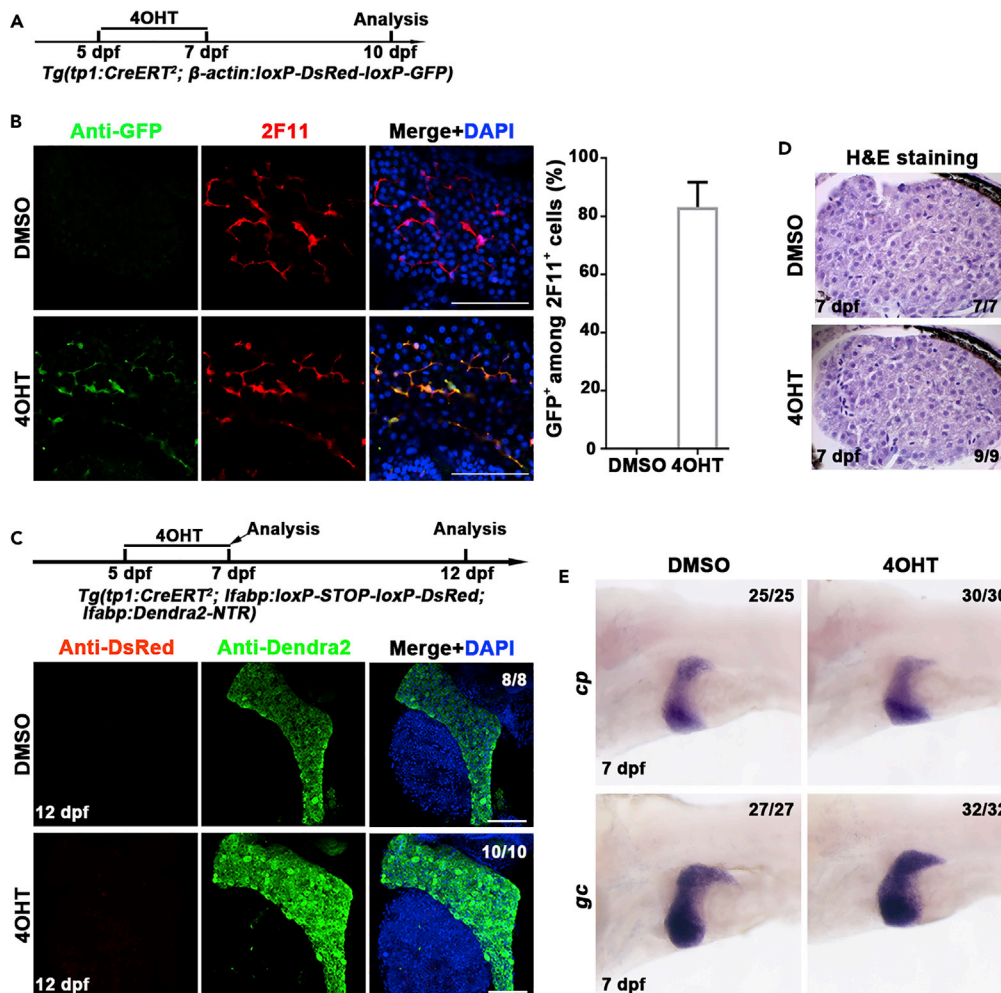
Figure 1. Establishment of the lineage tracing system specific for the detection of BEC-to-hepatocyte conversion

(A) Experimental scheme illustrating the stage of 4OHT treatment to double transgenic line, $Tg(tp1:CreERT^2; \beta\text{-}actin:loxP\text{-}DsRed\text{-}loxP\text{-}GFP)$ from 5 dpf to 7 dpf and analysis at 10 dpf.

(B) Immunostaining for 2F11 and GFP on livers (2D imaging) showing $tp1\text{-}CreER$ labels the 2F11-positive cholangiocytes specifically after 4OHT treatment. Nuclei were stained with DAPI (4',6-diamidino-2-phenylindole) (blue). Quantification of the percentage of GFP$^+$ among 2F11$^+$ cells in DMSO- (n = 5) and 4OHT (n = 6)-treated livers at 10 dpf.

(C) Experimental scheme illustrating the stage of 4OHT treatment to triple transgenic line $Tg(tp1:CreERT^2; lfabp: loxP\text{-}STOP\text{-}loxP\text{-}DsRed; lfabp:Dendra2\text{-}NTR)$ from 5 dpf to 7 dpf and analysis at 12 dpf. Immunostaining for DsRed and Dendra2 in livers (3D imaging) showing no DsRed positive cells in Dendra2$^+$ cells. Nuclei were stained with DAPI (blue).

(D) H&E staining images showing normal liver histologies at 7 dpf after DMSO and 4OHT treatment.

(E) Whole-mount *in situ* hybridization images showing the expression of *cp* and *gc* in DMSO and 4OHT treatment at 7 dpf. Scale bars: 100 μm. Data are represented as mean ±SEM (Standard Error of Mean) . See also Figure S1.

that the liver histology is unaffected by 4OHT (Figure 1D). Compared to DMSO treatment, the expressions of hepatocyte markers such as ceruloplasmin (*cp*) and vitamin D binding protein (*gc*) (Choi et al., 2017) in 4OHT treatment are unaltered (Figure 1E). These results exclude side effects of 4OHT such as induction of BEC-to-hepatocyte conversion or hepatotoxicity in this Cre/loxP lineage tracing system.

To avoid drawing conclusions based on a single promoter, a second promoter that is active in BECs, *keratin 18* (*krt18*), was used to generate the $Tg(krt18:CreERT^2)^{cq74}$ line (He et al., 2019). Of all, 88.7% of the 2F11-positive BECs were labeled with GFP when the $Tg(krt18:CreERT^2; \beta\text{-}actin:loxP\text{-}DsRed\text{-}loxP\text{-}GFP)$ double transgenic line was subjected to 4OHT treatment (Figure S2A). Immunostaining of GFP with 2F11 and Alcam showed that all GFP-positive cells were BECs (Figures S2B and S2C). While in the $Tg(krt18:CreERT^2;$

lfabp:loxP-STOP-loxP-DsRed; lfabp:Dendra2-NTR) triple transgenic line, five days after 4OHT treatment, all the hepatocytes were negative for DsRed (Figure S2D), again showing that 4OHT did not induce BEC-to-hepatocyte conversion. These results indicate that the *keratin 18* promoter is also applicable to trace the BEC-derived cells.

BECs are able to contribute to physiological hepatocyte homeostasis

To evaluate the contribution of BECs to hepatocyte homeostasis in zebrafish, we used the BEC-to-hepatocyte lineage tracing system *Tg(tp1:CreERT[2]; lfabp:loxP-STOP-loxP-DsRed; lfabp:Dendra2-NTR)* to trace the BEC-derived hepatocytes for 1 year and 2 years. Cre/loxP recombination will remove the *loxP*-flanked transcriptional Stop cassette so that all the descendants of BEC-derived hepatocytes will permanently express the genetic marker DsRed. This genetic labeling is heritable and irreversible. 4OHT treatment was applied from 5 dpf to 7 dpf, and the liver was analyzed 1 year or 2 years later (Figure 2A). Not all, but 25.4% of the total animals at one year exhibited BEC-to-hepatocyte conversion during liver homeostasis (Figure 2B, n=16/63). The ratio of BEC-derived, DsRed-positive hepatocytes was less than 3% in the major populations of these animals (Figure 2C, n=12/16), whereas minor populations exhibited more than 3% of hepatocytes derived from BECs (Figure 2C, n=4/16). At two years, the situation was similar to that at one year, with larger animal populations (n=24/70, 34.3%) obtaining the BEC-derived hepatocytes (Figures 2D and 2E). These data demonstrate that the BEC-derived hepatocytes do contribute to physiological hepatocyte homeostasis in some, but not all, zebrafish populations. More animals obtain the BEC-to-hepatocyte conversion if the tracing time is longer. However, the zebrafish populations with or without this conversion do not exhibit any difference in physiological status, fertility, and life span.

We then used the *keratin 18* line *Tg(krt18:CreERT[2]; lfabp:loxP-STOP-loxP-DsRed; lfabp:Dendra2-NTR)* to label the BECs at a later larval stage to validate the results obtained from the *tp1* promoter (Figure 3A). One year after 4OHT treatment, 31.1% of the total animals exhibited BEC-to-hepatocyte conversion during liver homeostasis (Figure 3B, n=14/45). The major populations of these animals obtained less than 3% of hepatocytes derived from BECs (Figure 3C, n=10/14), while minor populations gained more than 3% of hepatocytes converted from BECs (Figure 3C, n=4/14). All hepatocytes of the animals without 4OHT treatment were negative for DsRed (Figures 3B and 3C, n=18/18). These results confirm that the BEC-to-hepatocyte conversion occurs during hepatocyte homeostasis in zebrafish.

We tried to use the *Tg(lfabp:CreERT[2]; lfabp:loxP-STOP-loxP-DsRed; lfabp:Dendra2-NTR)* transgenic line, in which CreER was derived by the hepatocyte-specific promoter *lfabp*, to evaluate the contribution of hepatocyte self-renewal in liver homeostasis. 4OHT was applied from 5 dpf to 7 dpf and then removed (Figure S3A). One day after 4OHT withdrawal, although 96.8% of hepatocytes were positive for DsRed, the DMSO-treated control also showed DsRed in 8.1% of total hepatocytes (Figures S3B–S3D). At 1.5 months post-treatment, the ratios of DsRed-positive hepatocytes were 84.7% in the DMSO group and 99.0% in the 4OHT group (Figures S3E–S3G), which indicates that this line is only suitable for short-time tracing but not long-time tracing. These results indicate that our CreER transgenic line driven by the strong promoter *lfabp* is highly leaky so that it is not reliable for long-time lineage tracing of the self-renewal hepatocytes.

BECs do contribute to hepatocyte regeneration after extreme injury of the fibrotic liver

When a healthy liver undergoes extreme hepatocyte loss, liver regeneration occurs mainly via BEC trans-differentiation (Choi et al., 2014; He et al., 2014). This conclusion was confirmed by showing that 65.2% of regenerated hepatocytes originated from the *tp1*[+] BECs (Figures S4A–S4D).

To study the contribution of BECs after extreme injury of a fibrotic liver, which might be closer to the situation in the patients with liver diseases, we applied extreme loss of hepatocytes in the presence of fibrogenic insults (Huang et al., 2014, Huang et al., 2016). The *Tg(lfabp:Dendra2-NTR)[cq1]* transgenic larvae were exposed to 1.5% ethanol (EtOH) prior to the Mtz plus EtOH treatment (Figure 4A and Figure S5A). As previously described (Huang et al., 2014, Huang et al., 2016), the zebrafish developed hepatic steatosis with strong collagen expression in response to acute EtOH exposure (Figure 4B, arrows and S5B). The Sirius Red staining which is used to detect fibrosis in the liver (van der Helm et al., 2018) also showed fibrosis after extreme injury of EtOH-exposed liver (Figure S5C). After extreme injury of the fibrotic liver by Mtz, the 2F11-positive BECs started to co-express the hepatocyte marker Dendra2 from 8 hr post-Mtz treatment (R8h) on and maintained through R48h (Figure 4C). At R24h after Mtz plus EtOH treatment, most of the regenerating hepatocytes are double positive for 2F11 and Dendra2 (Figure 4D, arrows), which were not detected in the larvae without Mtz treatment (Figure 4D, arrowheads).
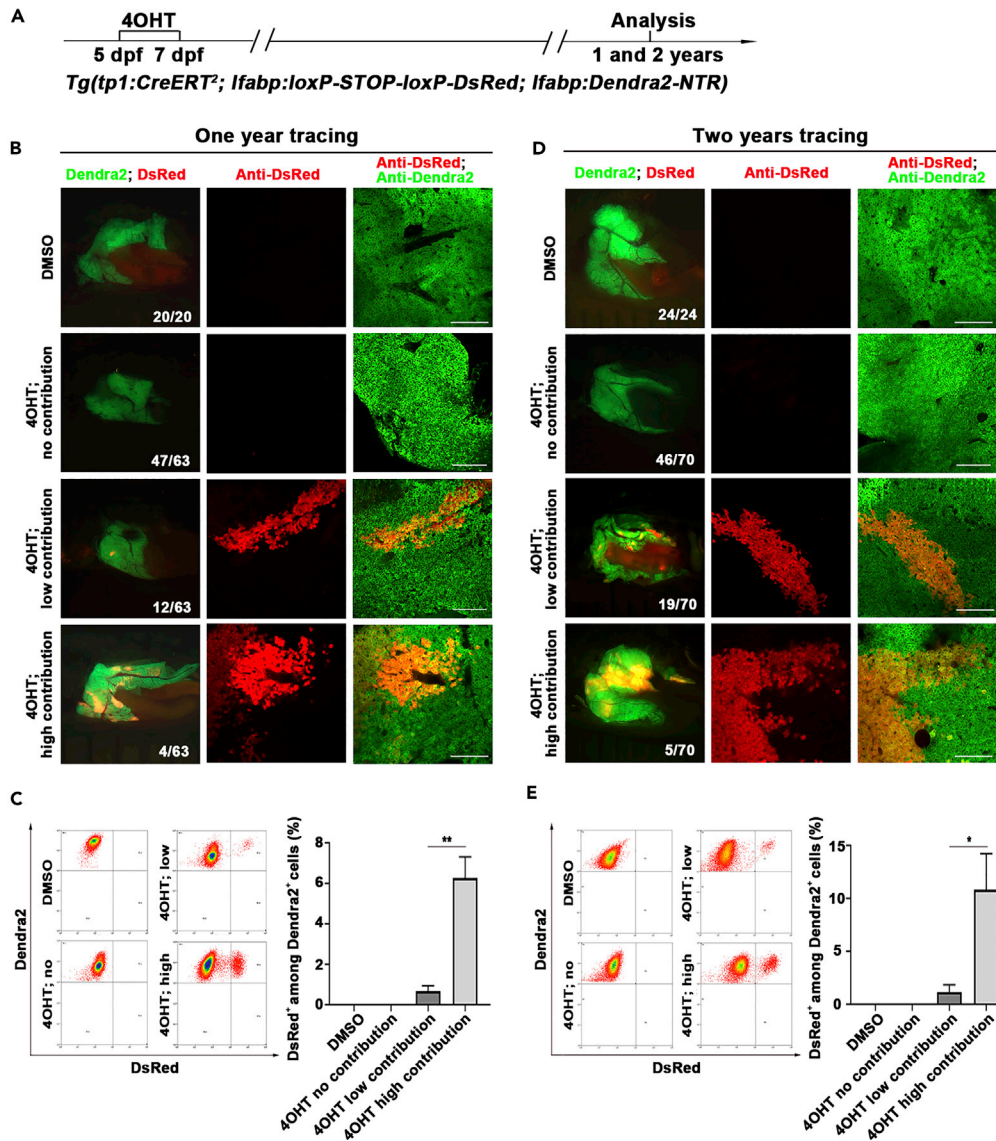
Figure 2. *Tp1*-positive BECs contribute to physiological hepatocyte homeostasis in a portion of zebrafish adults

(A) Experimental scheme illustrating the stage of 4OHT treatment to triple transgenic line *Tg(tp1:CreERT²; lfabp:loxP-STOP-loxP-DsRed; lfabp:Dendra2-NTR)* from 5 dpf to 7 dpf and analysis at 1 and 2 years.

(B) Live images showing the expression of Dendra2 and DsRed in the adult livers at 1 year. Co-immunostaining for Dendra2 and DsRed in the liver sections after DMSO and 4OHT treatment.

(C) Fluorescence activating cell sorter (FACS) analysis showing the ratio of DsRed+ among Dendra2+ cells in DMSO- and 4OHT-treated livers. Quantification of the percentage of DsRed+ among Dendra2+ cells in DMSO- (n=3) and 4OHT-treated (no contribution, n=3; low contribution, n=4; high contribution, n=3) livers at 1 year.

(D) Live images showing the expression of Dendra2 and DsRed in the adult livers at 2 years. Many clusters of DsRed+ cells among livers in 4OHT-treated groups. Co-immunostaining for Dendra2 and DsRed in the liver after DMSO and 4OHT treatment.

(E) Fluorescence activating cell sorter (FACS) analysis showing the ratio of DsRed+ among Dendra2+ cells in DMSO- and 4OHT-treated livers. Quantification of the percentage of DsRed+ among Dendra2+ cells in DMSO- (n=5) and 4OHT-treated (no contribution, n=4; low contribution, n=5; high contribution, n=3) livers at 2 years.

Numbers indicate the proportion of larvae exhibiting the expression shown. Asterisks indicate statistical significance: *p<0.05, **p<0.01, and p value was calculated by Student t tests. Scale bars: 100 μm. Data are represented as mean ±SEM.

To analyze the ratio of regenerating hepatocytes originated from BECs, we first checked whether the labeling efficiency of the Cre/loxP system was affected by the liver steatosis. Of all, 79.8% of the 2F11-positive BECs in the fibrotic liver were labeled by the Cre/loxP-activated GFP after 4OHT plus EtOH treatment from
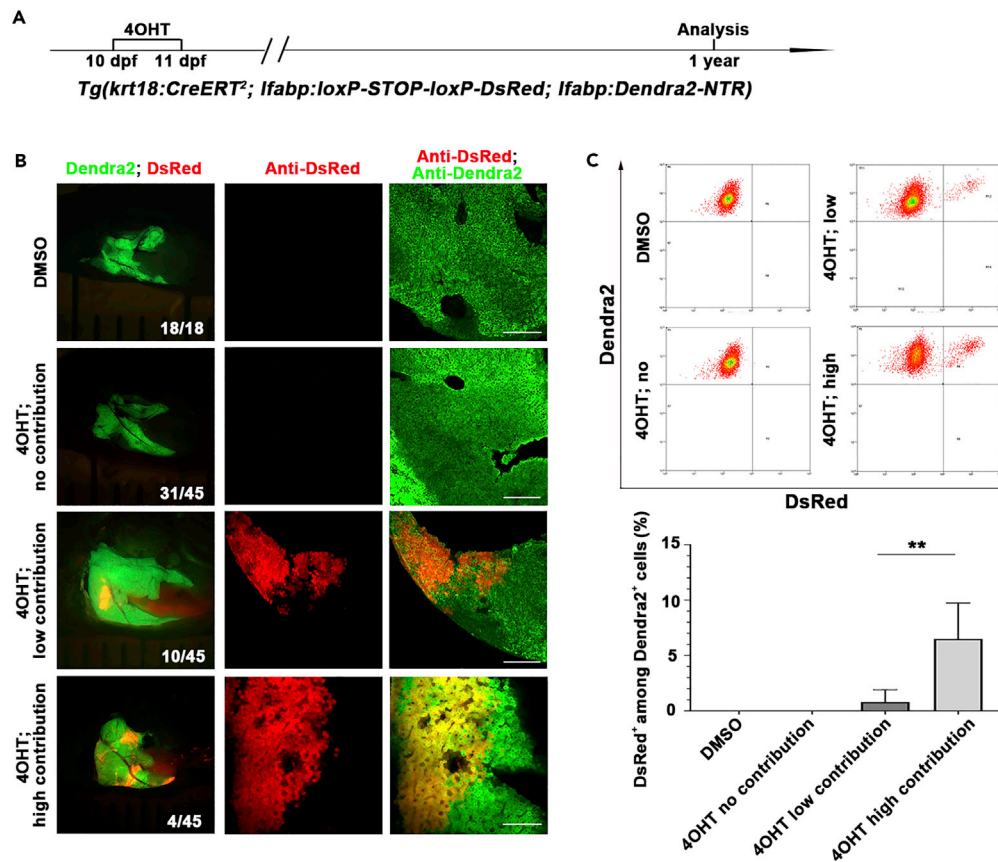
Figure 3. *Krt18*-positive BECs contribute to physiological hepatocyte homeostasis in a portion of zebrafish adults

(A) Experimental scheme illustrating the stage of 4OHT treatment to triple transgenic line *Tg(krt18:CreERT^2; lfabp:loxP-STOP-loxP-DsRed; lfabp:Dendra2-NTR)* from 10 dpf to 11 dpf and analysis at 1 year.

(B) Live images showing the expression of Dendra2 and DsRed in the adult livers at 1 year. Co-immunostaining for Dendra2 and DsRed in DMSO- and 4OHT-treated livers.

(C) Fluorescence activating cell sorter (FACS) analysis shows the ratio of DsRed$^+$ among Dendra2$^+$ cells in DMSO- and 4OHT-treated livers.

Quantification of the percentage of DsRed$^+$ among Dendra2$^+$ cells in DMSO- (n=5) and 4OHT-treated (no contribution, n=5; low contribution, n=8; high contribution, n=3) livers at 1 year.

Numbers indicate the proportion of larvae exhibiting the expression shown. Asterisks indicate statistical significance: **p<0.01, and p value was calculated by Student t tests. Scale bars: 100 μm. Data are represented as mean ±SEM. See also Figure S2.

4 dpf to 5 dpf (Figure 4E). Then, we used the BEC-to-hepatocyte lineage tracing system *Tg(tp1:CreERT^2; lfabp:loxP-STOP-loxP-DsRed; lfabp:Dendra2-NTR)* to induce liver steatosis and extreme hepatocyte loss (Figure 4F). At R72h, 60.3% of the newly formed hepatocytes were positive for DsRed (Figure 4F), suggesting that regeneration of fibrotic liver after extreme injury is primarily achieved through transdifferentiation of BECs. These results indicate that even in the case of a liver with a preexisting condition, the BEC conversion is still a regenerative mechanism available for the animal to use.

BECs fail to contribute to new hepatocytes after PH

Hepatocyte regeneration after PH has been reported to be mediated by the proliferation of residual hepatocytes in rodents (Grisham, 1962; Michalopoulos and DeFrances, 1997). We investigated the roles of BECs after PH in zebrafish (Figure 5A). At one day post-PH (dpp), although the 2F11-positive biliary ducts exhibited stress reactions such as dilations, cells double positive for 2F11 and Dendra2 were never observed (Figures 5B and 5C). At two weeks post-PH (wpp), the liver completely recovered (Figures 5D and 5E). The Cre/loxP-mediated lineage tracing showed a complete absence of the DsRed-positive hepatocyte (Figures 5E and 5F). These results indicate that the BEC-to-hepatocyte transdifferentiation does not occur after PH
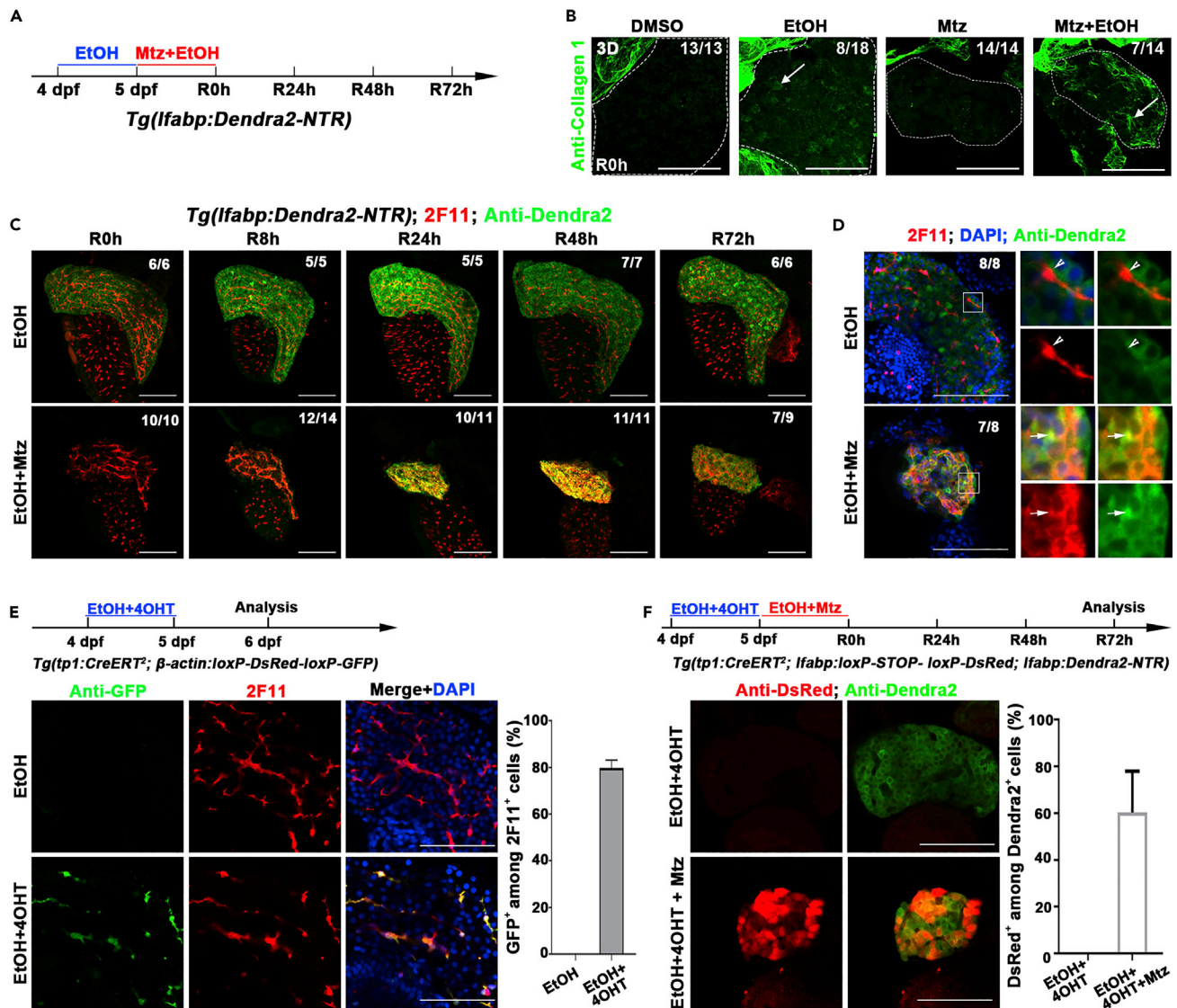
Figure 4. BECs act as the major contributor to hepatocyte regeneration after extreme injury to fibrotic liver

(A) Experimental scheme illustrating the stage of EtOH and Mtz treatment in transgenic line *Tg(lfabp:Dendra2-NTR)*.

(B) Confocal projection images (3D imaging) showing the staining of extracellular matrix protein collagen 1 in the liver region (dashed lines) after DMSO, EtOH, Mtz, and Mtz plus EtOH treatment at R0h (arrows).

(C) Confocal projection images (3D imaging) showing the co-immunostaining for Dendra2 and 2F11 in regenerating livers after EtOH and Mtz treatment from R0h to R72h.

(D) Single optical images showing the co-immunostaining for Dnedra2 and DsRed in regenerating livers at R24h. Most of the Dendra2$^+$ cells are 2F11 positive in Mtz and EtOH treatment (arrows). In EtOH treatment, the 2F11$^+$ and Dendra2$^+$ cells are not co-stained (arrowhead). Nuclei were stained with DAPI (blue).

(E) Experimental scheme illustrating the stage of 4OHT and EtOH treatment to double transgenic line, *Tg(tp1:CreERT²; β-actin:loxP-DsRed-loxP-GFP)*, from 4 dpf to 5 dpf and analysis at 6 dpf. Immunostaining for 2F11 and GFP on livers (2D imaging) showing *tp1-CreER* labels the 2F11-positive cholangiocytes specifically after 4OHT and EtOH treatment. Nuclei were stained with DAPI (blue). Quantification of the percentages of GFP$^+$ among 2F11+ hepatocytes (EtOH, n=5; EtOH+4OHT, n=8).

(F) Experimental scheme illustrating the stage of 4OHT, EtOH, and Mtz treatment to triple transgenic line *Tg(tp1:CreERT²; lfabp:loxP-STOP-loxP-DsRed; lfabp:Dendra2-NTR)* and analysis at R72h. Single optical images showing the co-immunostaining for DsRed and Dendra2 at R72h after 4OHT, EtOH, and Mtz treatment. Quantification of the percentage of the DsRed$^+$ among the Dendra2$^+$ cells in regenerating livers at R72h (EtOH+4OHT, n=10; EtOH+4OHT+Mtz, n=10).

Numbers indicate the proportion of larvae exhibiting the expression shown. Scale bars: 100 μm. Data are represented as mean ±SEM. See also Figures S4 and S5.
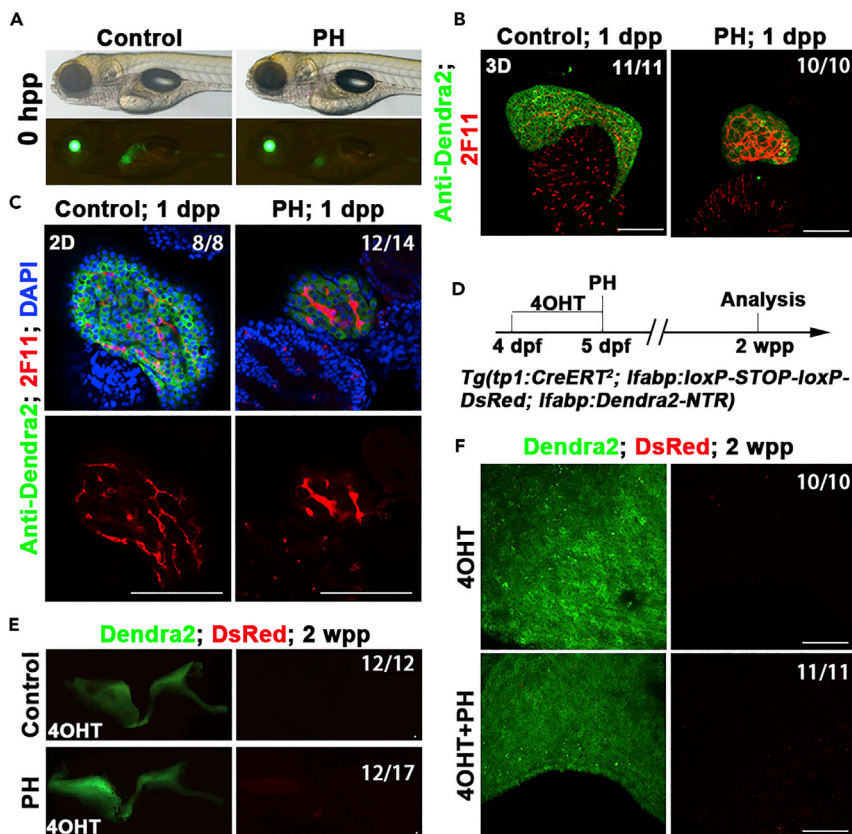
Figure 5. BECs fail to contribute to hepatocyte regeneration after PH

(A) Live images showing the liver (Green) after PH at 0 hpp.

(B) Confocal projection showing (3D imaging) the co-immunostaining for Dendra2 and 2F11 at 1 dpp.

(C) Single optical images showing the co-immunostaining for Dendra2 and 2F11 at 1 dpp. The 2F11[+] (BECs) were Dnedra2^{-}. Nuclei were stained with DAPI (blue).

(D) Experimental scheme illustrating the stage of 4OHT and PH and analysis at 2 wpp in triple transgenic line *Tg(tp1:CreERT[2]; lfabp:loxP-STOP-loxP-DsRed; lfabp:Dendra2-NTR)*.

(E) The confocal projection shows that no DsRed expression in regenerating livers at 2 wpp.

(F) The confocal projection (3D imaging) shows that no DsRed expression at 2 wpp in large magnification.

Numbers indicate the proportion of larvae exhibiting the expression shown. Scale bars: 100 μm. hpp: hours post-partial hepatectomy; dpp: days post-partial hepatectomy; wpp: weeks post-partial hepatectomy.

in zebrafish, in accordance with the results obtained in mammals (Brues and Marble, 1937; Michalopoulos, 2007; Miyaoka et al., 2012).

DISCUSSION

Physiological hepatocyte homeostasis in the liver is mainly dependent on hepatocyte self-renewal (Chen et al., 2013, 2020; Lin et al., 2018; Schaub et al., 2014; Sun et al., 2020; Tarlow et al., 2014b; Wang et al., 2015). But whether other cell types are capable of making contributions remains unclear. Although the Sox9-positive BECs have been reported to contribute to hepatocyte homeostasis (Furuyama et al., 2011), most of the recent studies in mammals and zebrafish propose against this conclusion (Carpentier et al., 2011; Espanol-Suner et al., 2012; Gao et al., 2018; Iverson et al., 2011; Malato et al., 2011; Rodrigo-Torres et al., 2014; Yanger et al., 2014). However, we have found that the lineage tracing systems used in these publications reporting negative results more or less fall into technical imperfections including insufficient sensitivity to detect micro-amount of the BEC-derived hepatocytes (Gao et al., 2018; Malato et al., 2011; Yanger et al., 2014), small sample size insufficient to distinguish heterogeneous individuals (Gao et al., 2018; Malato et al., 2011), short-term lineage tracing (Carpentier et al., 2011; Espanol-Suner et al., 2012; Iverson et al., 2011; Malato et al., 2011; Rodrigo-Torres et al., 2014), etc. To overcome these shortcomings in the analyses
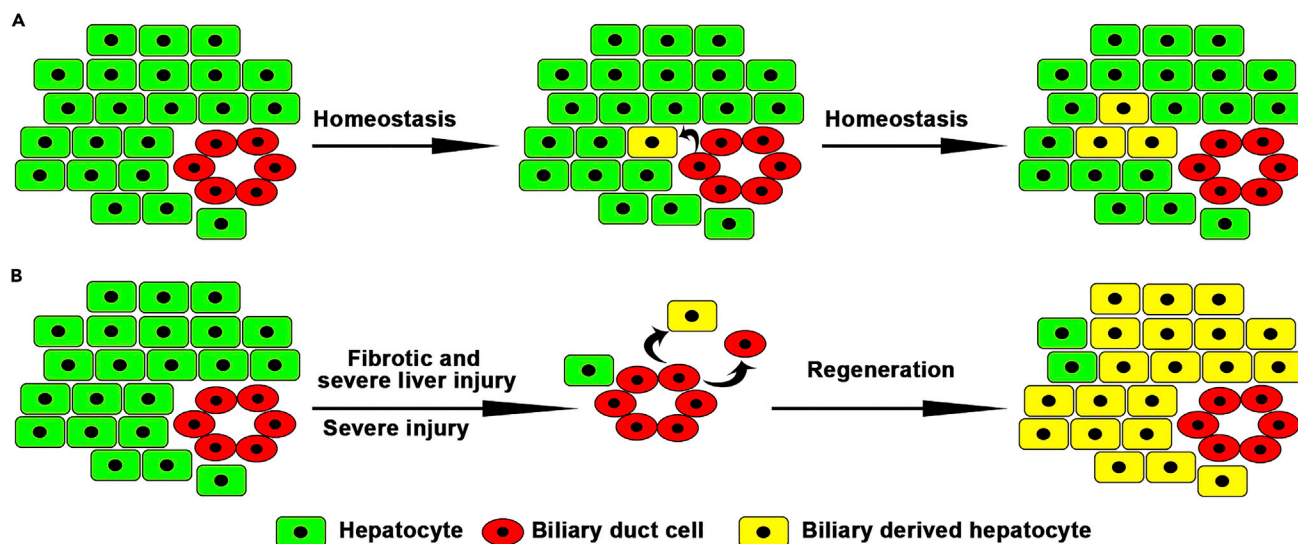
Figure 6. BECs contribute to physiological hepatocyte homeostasis and fibrotic and severe liver regeneration
(A) A subset of BECs contribute to physiological hepatocyte homeostasis.
(B) BEC transdifferentiations are the main cellular sources for fibrotic/severe and severe liver regeneration.

of BEC-to-hepatocyte conversion during hepatocyte homeostasis, we established a lineage tracing system in zebrafish specifically sensitive for the detection of the BEC-derived hepatocytes for more samples (up to 178 individuals) and longer time (up to two years) in the level of the whole liver. Through establishment and application of the lineage tracing system specific for the detection of the BEC-to-hepatocyte conversion, we conclude that BECs are capable of contributing to physiological hepatocyte homeostasis in a portion of zebrafish adult individuals, reassessing the function of BECs in liver growth and homeostasis.

BECs/cholangiocytes with different sizes or at different intrahepatic loci have been reported to be heterogeneous in protein expression and proliferation (Glaser et al., 2009). Their proliferative capacities are also heterogeneous during the thioacetamide-induced liver injury (Kamimoto et al., 2016). Our study recalls the heterogeneity of BECs and animal individuals. The BEC-derived hepatocytes distribute in clusters in the liver during hepatocyte homeostasis, implicating that BECs at different intrahepatic loci might obtain different potentials to convert into hepatocytes. Although healthy adult individuals do not exhibit any physiological differences, approximately a quarter to one-third, but not all, of them show detectable BEC-to-hepatocyte conversion during liver homeostasis. So, BECs do contribute to hepatocyte homeostasis.

Although the contribution of hepatocyte self-renewal to liver homeostasis has not been precisely evaluated in this study because of the leakiness of lfabp:CreER, we agree with the conclusion obtained by many studies that hepatocyte self-renewal is the major contributor to hepatocyte homeostasis (Chen et al., 2020; Matsumoto et al., 2020; Sun et al., 2020). Our results also disagree that the Sox9-positive BECs act as the major contributor to hepatocyte homeostasis (Furuyama et al., 2011). Nevertheless, our study shows that BECs, or sub-population of BECs, still maintain the potential to convert to hepatocytes and act as minor contributors to hepatocyte homeostasis under physiological circumstances (Figure 6A). Besides, our finding that the BEC-to-hepatocyte transdifferentiation does not occur after PH in zebrafish larvae is in accordance with the results obtained in mammals. So, the zebrafish larval PH model can be used to investigate more clinical problems with higher throughput screens.

Whether BECs contribute to hepatocyte homeostasis under physiological conditions remains unclear. In mice, lineage tracing for 6 months using a BAC transgenic *Sox9-CreERT²* has suggested that BECs do contribute to a portion of hepatocytes (Carpentier et al., 2011). Another study has used an "*in vivo* chronometer" system based on the albumin-Cre-mediated fluorescent conversion, suggesting that non-hepatocytes could act as continuous minor contributors to hepatocyte homeostasis (Iverson et al., 2011). These conclusions are consistent with our results, but other studies have drawn different conclusions. For example, the BEC lineage labeled by *Hnf1b-CreERT²* fails to convert to hepatocytes (Rodrigo-Torres

et al., 2014). However, the duration of lineage tracing in this study is relatively short, only two months (Rodrigo-Torres et al., 2014). Another example using hepatocytes labeled with the adeno-associated viral vector-incorporated Cre and ROSA (Gtrosa26)-EYFP (enhanced yellow fluorescent protein) reporter demonstrates that non-hepatocytic cells fail to contribute to hepatocyte homeostasis (Malato et al., 2011; Yanger et al., 2014). However, this labeling method is not sensitive enough to detect a minimal amount of EYFP-negative hepatocytes under the EYFP-positive background.

In zebrafish, maintenance of hepatocyte homeostasis has been reported to be entirely accomplished by hepatocyte self-renewal, without any contribution from BECs (Gao et al., 2018). However, this study by Gao et al. requires improvements in the following three aspects. First, Gao et al. labeled hepatocytes with yellow fluorescence and the hepatocyte-derived cells with green fluorescence. This labeling strategy is not sensitive enough to distinguish a very small amount of yellow$^+$ green$^-$ cells from the yellow$^+$ green$^+$ background. Gao et al. also labeled hepatocytes with yellow fluorescence and the BEC-derived cells with green fluorescence, which is also technically not sensitive enough to draw the conclusion that yellow and green fluorescences are completely non-overlapping. In contrast, in our study, only the BEC-derived hepatocytes exclusively exhibit red fluorescence, which is sensitive for detecting small amounts of cells. Second, our research indicates that a quarter to one-third of adult individuals show detectable BEC-to-hepatocyte transdifferentiation. On top of the first point above, the low sample size in the study by Gao et al (five adults) makes it even more difficult to detect the BEC-derived hepatocytes. Third, Gao et al. obtained results from sectioned liver samples. Due to the heterogeneity of BECs, it is likely that a portion of the sections misses the hepatocyte clusters derived from BECs. It is more rigorous to use full liver than liver sections for the study. All these three potential insufficiencies in the study by Gao et al study have been overcome in our study.

Regarding liver regeneration, this study together with previous studies (Choi et al., 2014; He et al., 2014; Huang et al., 2014) demonstrates that BEC transdifferentiation becomes the major contributor to the regenerating hepatocytes in both fibrotic and healthy zebrafish livers after extreme injury (Figure 6B). In mice, when the liver is damaged and in the meantime the proliferation of residual hepatocytes is inhibited, BECs do contribute to hepatocyte regeneration (Lu et al., 2015; Raven et al., 2017). All the studies above suggest the BEC-to-hepatocyte transdifferentiation as a conserved mechanism of liver regeneration in the vertebrate. In contrast to a healthy liver, the fibrotic liver analyzed in our study is closer to the clinical features of patients with liver diseases. BECs contribute to hepatocyte regeneration after extreme injury of fibrotic liver, providing potential clinical interest of BECs in the treatment of liver injuries.

Limitations of the study
Cholangiocytes with different sizes or at different intrahepatic loci may be heterogeneous, and some of the BECs can contribute to hepatocytes in liver homeostasis. However, the detailed cellular and mlecular mechanisms underly the heterogeneous of BECs need to be addressed further.

Resource availability
Lead contact
Further information and requests for resources and reagents should be directed to and will be fulfilled by the lead contact, Jianbo He (hejianbo@swu.edu.cn).

Material availability
All unique/stable reagents generated in this study are available to qualified researchers via contacting the lead contact.

Data and code availability
The published article includes all data sets generated or analyzed during this study.

METHODS
All methods can be found in the accompanying Transparent methods supplemental file.

SUPPLEMENTAL INFORMATION
Supplemental information can be found online at https://doi.org/10.1016/j.isci.2021.102142.

AUTHOR CONTRIBUTIONS

J.H. and L.L. designed the experimental strategy, analyzed data, and wrote the manuscript. J.C. performed liver injury and regeneration experiments. R.N. performed the FACS (Fluorescence activated Cell Sorting). Q.Y. performed tissue sections. W.Z. performed all the other experiments.

DECLARATION OF INTERESTS

The authors declare no competing interests.

REFERENCES

Bralet, M.P., Branchereau, S., Brechot, C., and Ferry, N. (1994). Cell lineage study in the liver using retroviral mediated gene transfer. Evidence against the streaming of hepatocytes in normal liver. Am. J. Pathol. *144*, 896–905.

Brues, A.M., and Marble, B.B. (1937). An analysis of mitosis in liver restoration. J. Exp. Med. *65*, 15–27.

Carpentier, R., Suner, R.E., van Hul, N., Kopp, J.L., Beaudry, J.B., Cordi, S., Antoniou, A., Raynaud, P., Lepreux, S., Jacquemin, P., et al. (2011). Embryonic ductal plate cells give rise to cholangiocytes, periportal hepatocytes, and adult liver progenitor cells. Gastroenterology *141*, 1432–1438, 1438.e1-4.

Chen, F., Jimenez, R.J., Sharma, K., Luu, H.Y., Hsu, B.Y., Ravindranathan, A., Stohr, B.A., and Willenbring, H. (2020). Broad distribution of hepatocyte proliferation in liver homeostasis and regeneration. Cell Stem Cell *26*, 27–33 e24.

Chen, Y.H., Chang, M.H., Chien, C.S., Wu, S.H., Yu, C.H., and Chen, H.L. (2013). Contribution of mature hepatocytes to small hepatocyte-like progenitor cells in retrorsine-exposed rats with chimeric livers. Hepatology *57*, 1215–1224.

Choi, T.-Y., Khaliq, M., Tsurusaki, S., Ninov, N., Stainier, D.Y.R., Tanaka, M., and Shin, D. (2017). Bone morphogenetic protein signaling governs biliary-driven liver regeneration in zebrafish through tbx2b and id2a. Hepatology *66*, 1616–1630.

Choi, T.Y., Ninov, N., Stainier, D.Y., and Shin, D. (2014). Extensive conversion of hepatic biliary epithelial cells to hepatocytes after near total loss of hepatocytes in zebrafish. Gastroenterology *146*, 776–788.

Deng, X., Zhang, X., Li, W., Feng, R.-X., Li, L., Yi, G.-R., Zhang, X.-N., Yin, C., Yu, H.-Y., Zhang, J.-P., et al. (2018). Chronic liver injury induces conversion of biliary epithelial cells into hepatocytes. Cell Stem Cell *23*, 114–122.e3.

Duncan, A.W., Dorrell, C., and Grompe, M. (2009). Stem cells and liver regeneration. Gastroenterology *137*, 466–481.

Espanol-Suner, R., Carpentier, R., Van Hul, N., Legry, V., Achouri, Y., Cordi, S., Jacquemin, P., Lemaigre, F., and Leclercq, I.A. (2012). Liver progenitor cells yield functional hepatocytes in response to chronic liver injury in mice. Gastroenterology *143*, 1564–1575.e7.

Evarts, R.P., Nagy, P., Marsden, E., and Thorgeirsson, S.S. (1987). A precursor-product relationship exists between oval cells and hepatocytes in rat liver. Carcinogenesis *8*, 1737–1740.

Fausto, N., and Campbell, J.S. (2003). The role of hepatocytes and oval cells in liver regeneration and repopulation. Mech. Dev. *120*, 117–130.

Fellous, T.G., Islam, S., Tadrous, P.J., Elia, G., Kocher, H.M., Bhattacharya, S., Mears, L., Turnbull, D.M., Taylor, R.W., Greaves, L.C., et al. (2009). Locating the stem cell niche and tracing hepatocyte lineages in human liver. Hepatology *49*, 1655–1663.

Furuyama, K., Kawaguchi, Y., Akiyama, H., Horiguchi, M., Kodama, S., Kuhara, T., Hosokawa, S., Elbahrawy, A., Soeda, T., Koizumi, M., et al. (2011). Continuous cell supply from a Sox9-expressing progenitor zone in adult liver, exocrine pancreas and intestine. Nat. Genet. *43*, 34–41.

Gadd, V.L., Aleksieva, N., and Forbes, S.J. (2020). Epithelial plasticity during liver injury and regeneration. Cell Stem Cell *27*, 557–573.

Gao, C., Zhu, Z., Gao, Y., Lo, L.J., Chen, J., Luo, L., and Peng, J. (2018). Hepatocytes in a normal adult liver are derived solely from the embryonic hepatocytes. J. Genet. Genomics *45*, 173–175.

Glaser, S.S., Gaudio, E., Rao, A., Pierce, L.M., Onori, P., Franchitto, A., Francis, H.L., Dostal, D.E., Venter, J.K., DeMorrow, S., et al. (2009). Morphological and functional heterogeneity of

the mouse intrahepatic biliary epithelium. Lab. Invest. *89*, 456–469.

Grisham, J.W. (1962). A morphologic study of deoxyribonucleic acid synthesis and cell proliferation in regenerating rat liver; autoradiography with thymidine-H3. Cancer Res. *22*, 842–849.

He, J., Chen, J., Wei, X., Leng, H., Mu, H., Cai, P., and Luo, L. (2019). Mammalian target of rapamycin complex 1 signaling is required for the dedifferentiation from biliary cell to bipotential progenitor cell in zebrafish liver regeneration. Hepatology (Baltimore, Md) *70*, 2092–2106.

He, J., Lu, H., Zou, Q., and Luo, L. (2014). Regeneration of liver after extreme hepatocyte loss occurs mainly via biliary transdifferentiation in zebrafish. Gastroenterology *146*, 789–800.e8.

Huang, M., Chang, A., Choi, M., Zhou, D., Anania, F.A., and Shin, C.H. (2014). Antagonistic interaction between Wnt and Notch activity modulates the regenerative capacity of a zebrafish fibrotic liver model. Hepatology *60*, 1753–1766.

Huang, M., Xu, J., and Shin, C.H. (2016). Development of an ethanol-induced fibrotic liver model in zebrafish to study progenitor cell-mediated hepatocyte regeneration. J. Vis. Exp. 54002.

Huch, M., Dorrell, C., Boj, S.F., van Es, J.H., Li, V.S.W., van de Wetering, M., Sato, T., Hamer, K., Sasaki, N., Finegold, M.J., et al. (2013). In vitro expansion of single Lgr5(+) liver stem cells induced by Wnt-driven regeneration. Nature *494*, 247–250.

Iverson, S.V., Comstock, K.M., Kundert, J.A., and Schmidt, E.E. (2011). Contributions of new hepatocyte lineages to liver growth, maintenance, and regeneration in mice. Hepatology *54*, 655–663.

Kamimoto, K., Kaneko, K., Kok, C.Y., Okada, H., Miyajima, A., and Itoh, T. (2016). Heterogeneity and stochastic growth regulation of biliary

epithelial cells dictate dynamic epithelial tissue remodeling. Elife 5, e15034.

Kennedy, S., Rettinger, S., Flye, M.W., and Ponder, K.P. (1995). Experiments in transgenic mice show that hepatocytes are the source for postnatal liver growth and do not stream. Hepatology 22, 160–168.

Ko, S., Choi, T.-Y., Russell, J.O., So, J., Monga, S.P.S., and Shin, D. (2016). Bromodomain and extraterminal (BET) proteins regulate biliary-driven liver regeneration. J. Hepatol. 64, 316–325.

Ko, S., Russell, J.O., Molina, L.M., and Monga, S.P. (2020). Liver progenitors and adult cell plasticity in hepatic injury and repair: knowns and unknowns. Annu. Rev. Pathol. 15, 23–50.

Ko, S., Russell, J.O., Tian, J., Gao, C., Kobayashi, M., Feng, R., Yuan, X., Shao, C., Ding, H., Poddar, M., et al. (2019). Hdac1 regulates differentiation of bipotent liver progenitor cells during regeneration via Sox9b and Cdk8. Gastroenterology 156, 187–202.e14.

Li, W., Li, L., and Hui, L. (2020). Cell plasticity in liver regeneration. Trends Cell Biol. 30, 329–338.

Lin, S., Nascimento, E.M., Gajera, C.R., Chen, L., Neuhofer, P., Garbuzov, A., Wang, S., and Artandi, S.E. (2018). Distributed hepatocytes expressing telomerase repopulate the liver in homeostasis and injury. Nature 556, 244–248.

Liu, J., Bressan, M., Hassel, D., Huisken, J., Staudt, D., Kikuchi, K., Poss, K.D., Mikawa, T., and Stainier, D.Y. (2010). A dual role for ErbB2 signaling in cardiac trabeculation. Development 137, 3867–3875.

Lu, W.Y., Bird, T.G., Boulter, L., Tsuchiya, A., Cole, A.M., Hay, T., Guest, R.V., Wojtacha, D., Man, T.Y., Mackinnon, A., et al. (2015). Hepatic progenitor cells of biliary origin with liver repopulation capacity. Nat. Cell Biol. 17, 971–983.

Malato, Y., Naqvi, S., Schurmann, N., Ng, R., Wang, B., Zape, J., Kay, M.A., Grimm, D., and Willenbring, H. (2011). Fate tracing of mature hepatocytes in mouse liver homeostasis and regeneration. J. Clin. Invest. 121, 4850–4860.

Manco, R., Clerbaux, L.-A., Verhulst, S., Bou Nader, M., Sempoux, C., Ambroise, J., Bearzatto, B., Gala, J.L., Horsmans, Y., van Grunsven, L., et al. (2019). Reactive cholangiocytes differentiate into proliferative hepatocytes with efficient DNA repair in mice with chronic liver injury. J. Hepatol. 70, 1180–1191.

Matsumoto, T., Wakefield, L., Tarlow, B.D., and Grompe, M. (2020). In vivo lineage tracing of polyploid hepatocytes reveals extensive proliferation during liver regeneration. Cell Stem Cell 26, 34–47.e3.

Michalopoulos, G.K. (2007). Liver regeneration. J. Cell Physiol. 213, 286–300.

Michalopoulos, G.K., Barua, L., and Bowen, W.C. (2005). Transdifferentiation of rat hepatocytes into biliary cells after bile duct ligation and toxic biliary injury. Hepatology 41, 535–544.

Michalopoulos, G.K., and DeFrances, M.C. (1997). Liver regeneration. Science 276, 60–66.

Miyajima, A., Tanaka, M., and Itoh, T. (2014). Stem/progenitor cells in liver development, homeostasis, regeneration, and reprogramming. Cell Stem Cell 14, 561–574.

Miyaoka, Y., Ebato, K., Kato, H., Arakawa, S., Shimizu, S., and Miyajima, A. (2012). Hypertrophy and unconventional cell division of hepatocytes underlie liver regeneration. Curr. Biol. 22, 1166–1175.

Raven, A., Lu, W.Y., Man, T.Y., Ferreira-Gonzalez, S., O'Duibhir, E., Dwyer, B.J., Thomson, J.P., Meehan, R.R., Bogorad, R., Koteliansky, V., et al. (2017). Cholangiocytes act as facultative liver stem cells during impaired hepatocyte regeneration. Nature 547, 350–354.

Rodrigo-Torres, D., Affo, S., Coll, M., Morales-Ibanez, O., Millan, C., Blaya, D., Alvarez-Guaita, A., Rentero, C., Lozano, J.J., Maestro, M.A., et al. (2014). The biliary epithelium gives rise to liver progenitor cells. Hepatology 60, 1367–1377.

Rollins, M.F., van der Heide, D.M., Weisend, C.M., Kundert, J.A., Comstock, K.M., Suvorova, E.S., Capecchi, M.R., Merrill, G.F., and Schmidt, E.E. (2010). Hepatocytes lacking thioredoxin reductase 1 have normal replicative potential during development and regeneration. J. Cell Sci. 123, 2402–2412.

Russell, J.O., Ko, S., Monga, S.P., and Shin, D. (2019). Notch inhibition promotes differentiation of liver progenitor cells into hepatocytes via repression in zebrafish. Stem Cells Int. 2019, 8451282.

Sakaguchi, T.F., Sadler, K.C., Crosnier, C., and Stainier, D.Y.R. (2008). Endothelial signals modulate hepatocyte apicobasal polarization in zebrafish. Curr. Biol. 18, 1565–1571.

Sato, K., Marzioni, M., Meng, F., Francis, H., Glaser, S., and Alpini, G. (2019). Ductular reaction in liver diseases: pathological mechanisms and translational significances. Hepatology 69, 420–430.

Schaub, J.R., Malato, Y., Gormond, C., and Willenbring, H. (2014). Evidence against a stem cell origin of new hepatocytes in a common mouse model of chronic liver injury. Cell Rep. 8, 933–939.

So, J., Kim, M., Lee, S.-H., Ko, S., Lee, D.A., Park, H., Azuma, M., Parsons, M.J., Prober, D., and Shin, D. (2020). Attenuating the EGFR-ERK-SOX9 axis promotes liver progenitor cell-mediated liver regeneration in zebrafish. Hepatology. https://doi.org/10.1002/hep.31437.

Stanger, B.Z. (2015). Cellular homeostasis and repair in the mammalian liver. Annu. Rev. Physiol. 77, 179–200.

Sun, T., Pikiolek, M., Orsini, V., Bergling, S., Holwerda, S., Morelli, L., Hoppe, P.S., Planas-Paz, L., Yang, Y., Ruffner, H., et al. (2020). AXIN2(+) pericentral hepatocytes have limited contributions to liver homeostasis and regeneration. Cell Stem Cell 26, 97–107.e6.

Tanimizu, N., Nishikawa, Y., Ichinohe, N., Akiyama, H., and Mitaka, T. (2014). Sry HMG box protein 9-positive (Sox9(+)) epithelial cell adhesion molecule-negative (EpCAM(-))

biphenotypic cells derived from hepatocytes are involved in mouse liver regeneration. J. Biol. Chem. 289, 7589–7598.

Tarlow, B.D., Finegold, M.J., and Grompe, M. (2014a). Clonal tracing of Sox9+ liver progenitors in mouse oval cell injury. Hepatology 60, 278–289.

Tarlow, B.D., Pelz, C., Naugler, W.E., Wakefield, L., Wilson, E.M., Finegold, M.J., and Grompe, M. (2014b). Bipotential adult liver progenitors are derived from chronically injured mature hepatocytes. Cell Stem Cell 15, 605–618.

van der Helm, D., Groenewoud, A., de Jonge-Muller, E.S.M., Barnhoorn, M.C., Schoonderwoerd, M.J.A., Coenraad, M.J., Hawinkels, L., Snaar-Jagalska, B.E., van Hoek, B., and Verspaget, H.W. (2018). Mesenchymal stromal cells prevent progression of liver fibrosis in a novel zebrafish embryo model. Sci. Rep. 8, 16005.

Venkatachalam, A.B., Thisse, C., Thisse, B., and Wright, J.M. (2009). Differential tissue-specific distribution of transcripts for the duplicated fatty acid-binding protein 10 (fabp10) genes in embryos, larvae and adult zebrafish (Danio rerio). FEBS J. 276, 6787–6797.

Wang, B., Zhao, L., Fish, M., Logan, C.Y., and Nusse, R. (2015). Self-renewing diploid Axin2(+) cells fuel homeostatic renewal of the liver. Nature 524, 180–185.

Wang, X., Foster, M., Al-Dhalimy, M., Lagasse, E., Finegold, M., and Grompe, M. (2003). The origin and liver repopulating capacity of murine oval cells. Proc. Natl. Acad. Sci. U S A 100, 11881–11888.

Wang, Y., Rovira, M., Yusuff, S., and Parsons, M.J. (2011). Genetic inducible fate mapping in larval zebrafish reveals origins of adult insulin-producing beta-cells. Development 138, 609–617.

Yanger, K., Knigin, D., Zong, Y., Maggs, L., Gu, G., Akiyama, H., Pikarsky, E., and Stanger, B.Z. (2014). Adult hepatocytes are generated by self-duplication rather than stem cell differentiation. Cell Stem Cell 15, 340–349.

Yanger, K., Zong, Y., Maggs, L.R., Shapira, S.N., Maddipati, R., Aiello, N.M., Thung, S.N., Wells, R.G., Greenbaum, L.E., and Stanger, B.Z. (2013). Robust cellular reprogramming occurs spontaneously during liver regeneration. Genes Dev. 27, 719–724.

Yovchev, M.I., Grozdanov, P.N., Zhou, H., Racherla, H., Guha, C., and Dabeva, M.D. (2008). Identification of adult hepatic progenitor cells capable of repopulating injured rat liver. Hepatology 47, 636–647.

Zaret, K.S., and Grompe, M. (2008). Generation and regeneration of cells of the liver and pancreas. Science 322, 1490–1494.

Zhang, D., Golubkov, V.S., Han, W., Correa, R.G., Zhou, Y., Lee, S., Strongin, A.Y., and Dong, P.D. (2014). Identification of Annexin A4 as a hepatopancreas factor involved in liver cell survival. Dev. Biol. 395, 96–110.
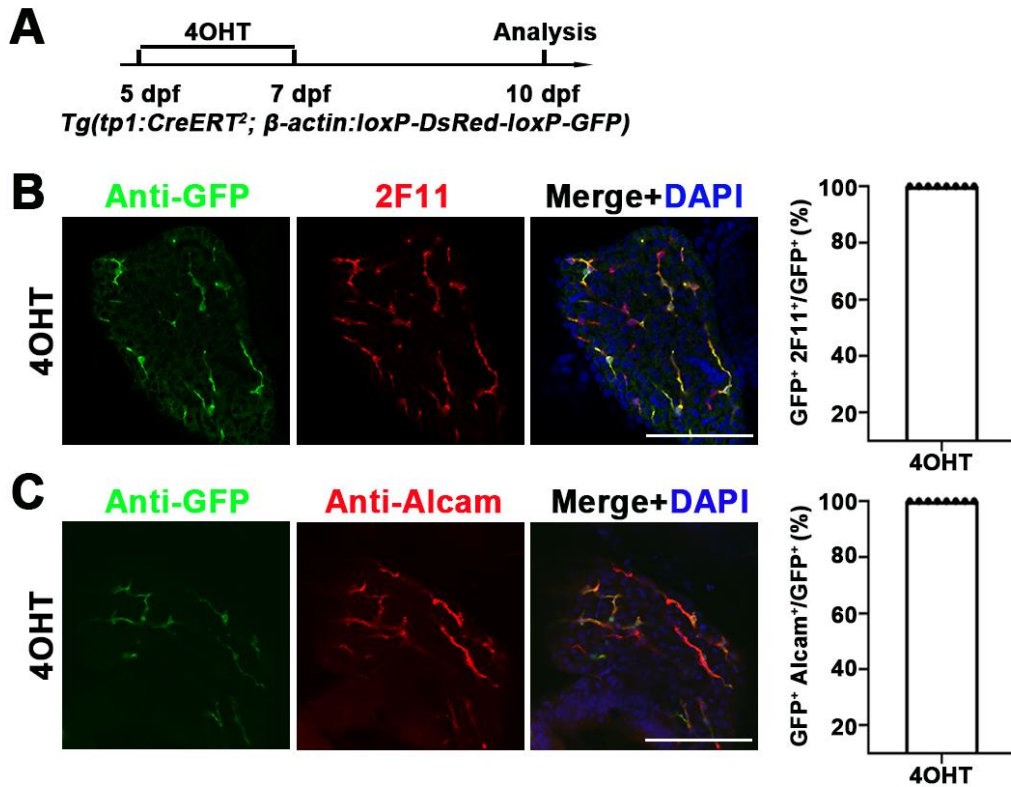
Supplemental Information

Contributions of biliary epithelial

cells to hepatocyte homeostasis

and regeneration in zebrafish

Wenfeng Zhang, Jingying Chen, Rui Ni, Qifen Yang, Lingfei Luo, and Jianbo He

SUPPLEMENTAL FIGURE AND LEGEND

He_Figure S1

Figure S1. Establishment of lineage tracing system of physiological BEC-to-hepatocyte conversion using the *tp1* promoter. Related to Figure 1 and Figure 2. (**A**) Experimental scheme illustrating the stage of 4OHT treatment to double transgenic line, *Tg(tp1:CreERT2; β-actin:loxP-DsRed-loxP-GFP)* from 5 dpf to 7 dpf and analysis at 10 dpf. (**B**) Immunostaining for 2F11 and GFP on livers (2D imaging) showing *tp1-CreER* labels the 2F11 positive cholangiocytes specifically after 4OHT treatment. Nuclei were stained with DAPI (blue). Quantification of the percentage of the GFP+2F11+ among the GFP+ cells in 4OHT (n=8) treated livers. (**C**) Immunostaining for Alcam and GFP on livers (2D imaging) showing *tp1-CreER* labels the Alcam positive cholangiocytes specifically after 4OHT treatment. Nuclei were stained with DAPI (blue). Quantification of the percentage of the GFP+Alcam+ among the GFP+ cells in 4OHT (n=8) treated livers. Scale bars: 100 μm. Data are represented as mean ±SEM.
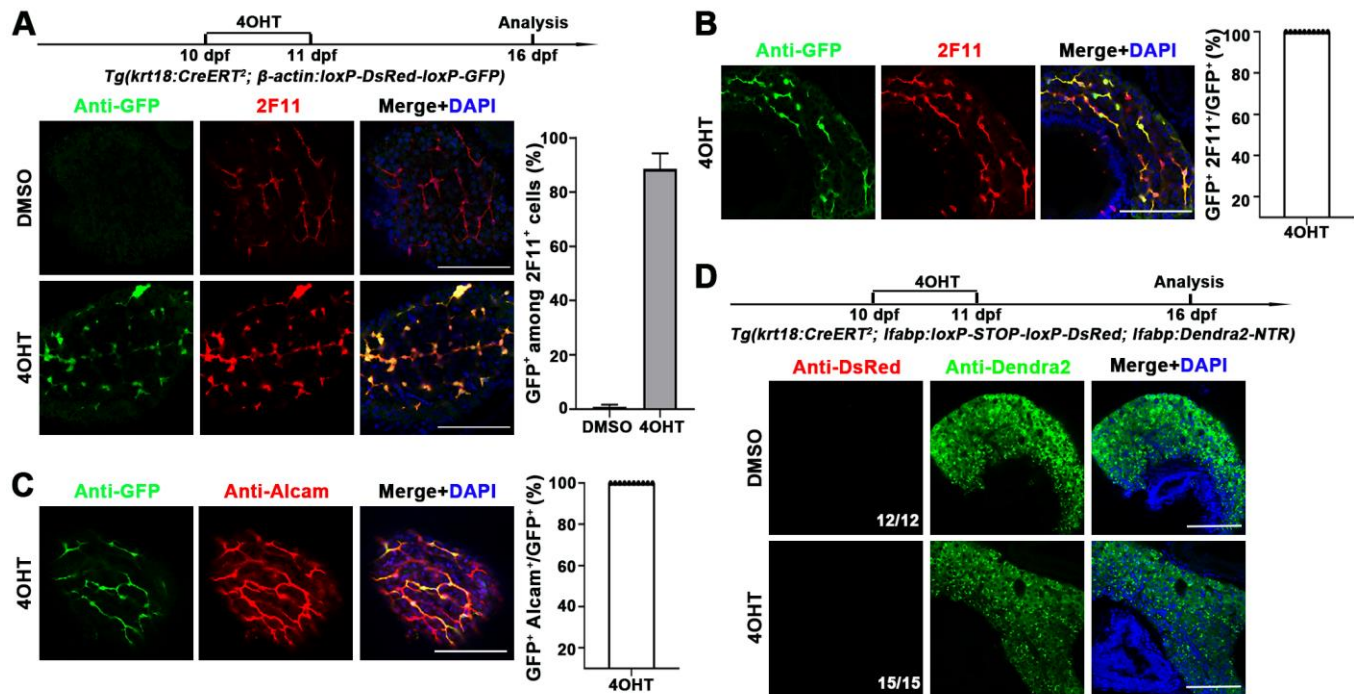
He_Figure S2

Figure S2. Establishment of lineage tracing system of physiological BEC-to-hepatocyte conversion using the *krt18* promoter. Related to Figure 3. (**A**) Experimental scheme illustrating the stage of 4OHT treatment to double transgenic line, *Tg(krt18:CreERT², β-actin:loxP-DsRed-loxP-GFP)* from 10 dpf to 11 dpf and analysis at 16 dpf. Immunostaining for 2F11 and GFP on livers (2D imaging) showing *krt18-CreER* labels the 2F11 positive cholangiocytes specifically after 4OHT treatment. Nuclei were stained with DAPI (blue). Quantification of the percentage of the GFP⁺ among the 2F11⁺ cells in DMSO (n=6) and 4OHT (n=6) treated livers. (**B**) Immunostaining for 2F11 and GFP on livers (2D imaging) showing *krt18-CreER* labels the 2F11 positive cholangiocytes specifically after 4OHT treatment. Nuclei were stained with DAPI (blue). Quantification of the percentage of the GFP⁺2F11⁺ among the GFP⁺ cells in 4OHT (n=10) treated livers; (**C**) Immunostaining for Alcam and GFP on livers (2D imaging) showing *krt18-CreER* labels the Alcam positive cholangiocytes specifically after 4OHT treatment. Nuclei were stained with DAPI (blue). Quantification of the percentage of the GFP⁺Alcam⁺ among the GFP⁺ cells in 4OHT (n=10) treated livers. (**D**) Experimental scheme illustrating the stage of 4OHT treatment to triple transgenic line *Tg(krt18:CreERT²; lfabp: loxP-STOP-loxP-DsRed; lfabp:Dendra2-NTR)* from 10 dpf to 11 dpf and analysis at 16 dpf. Immunostaining for DsRed and Dendra2 in livers (2D imaging) showing no DsRed⁺Dendra⁺ cells. Nuclei were stained with DAPI (blue). Scale bars: 100 μm. Data are represented as mean ±SEM.
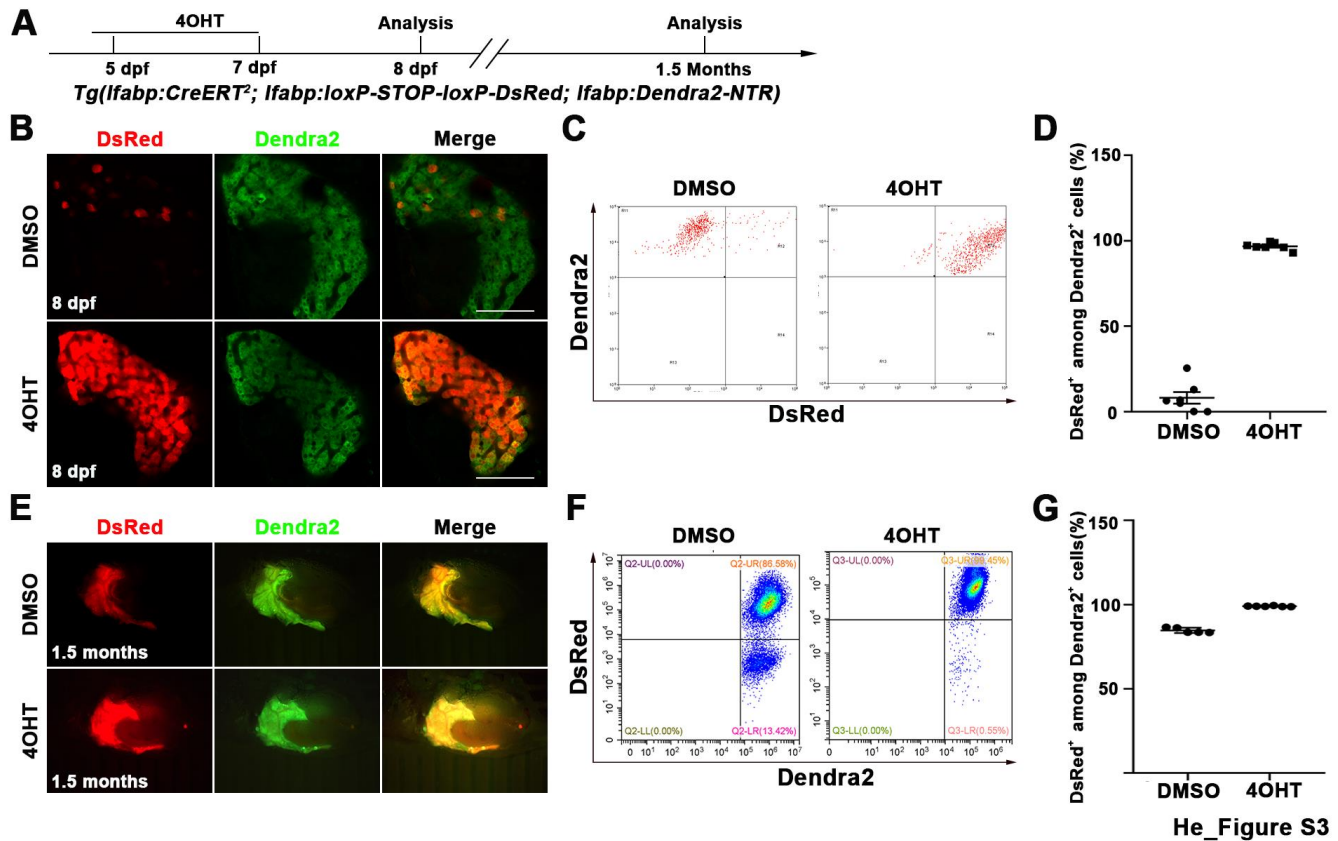
Figure S3. Transgenic line *Tg(Ifabp:CreERT²)* shows high leakiness in long term lineage tracing. Related to Figure 2 and Figure 3. (**A**) Experimental scheme illustrating the stage of 4OHT treatment to triple transgenic line *Tg(Ifabp:CreERT²; Ifabp:loxP-STOP-loxP-DsRed; Ifabp:Dendra2-NTR)* and analysis at 8 dpf and 1.5 months, respectively. (**B**) Single-optical images showing a low level of "leaky" (low level of DsRed⁺ in Dendra2⁺ cells) in early development (8 dpf) in DMSO treatment. (**C**) Fluorescence Activating Cell Sorter (FACS) analysis showing the ratio of DsRed⁺ among Dendra2⁺ cells in DMSO and 4OHT treated livers. (**D**) Quantification of the percentages of DsRed⁺ among Dendra2⁺ hepatocytes (DMSO, n=7; 4OHT, n=7). (**E**) Live images showing strong DsRed expression in livers at 1.5 months in DMSO and 4OHT treatment. (**F**) FACS analysis showing the ratio of DsRed⁺ among Dendra2⁺ cells in DMSO and 4OHT treated livers at 1.5 months. (**G**) Quantification of the percentages of DsRed⁺ among Dendra2⁺ hepatocytes (DMSO, n=5; 4OHT, n=6). Scale bars: 100 μm. Data are represented as mean ±SEM.
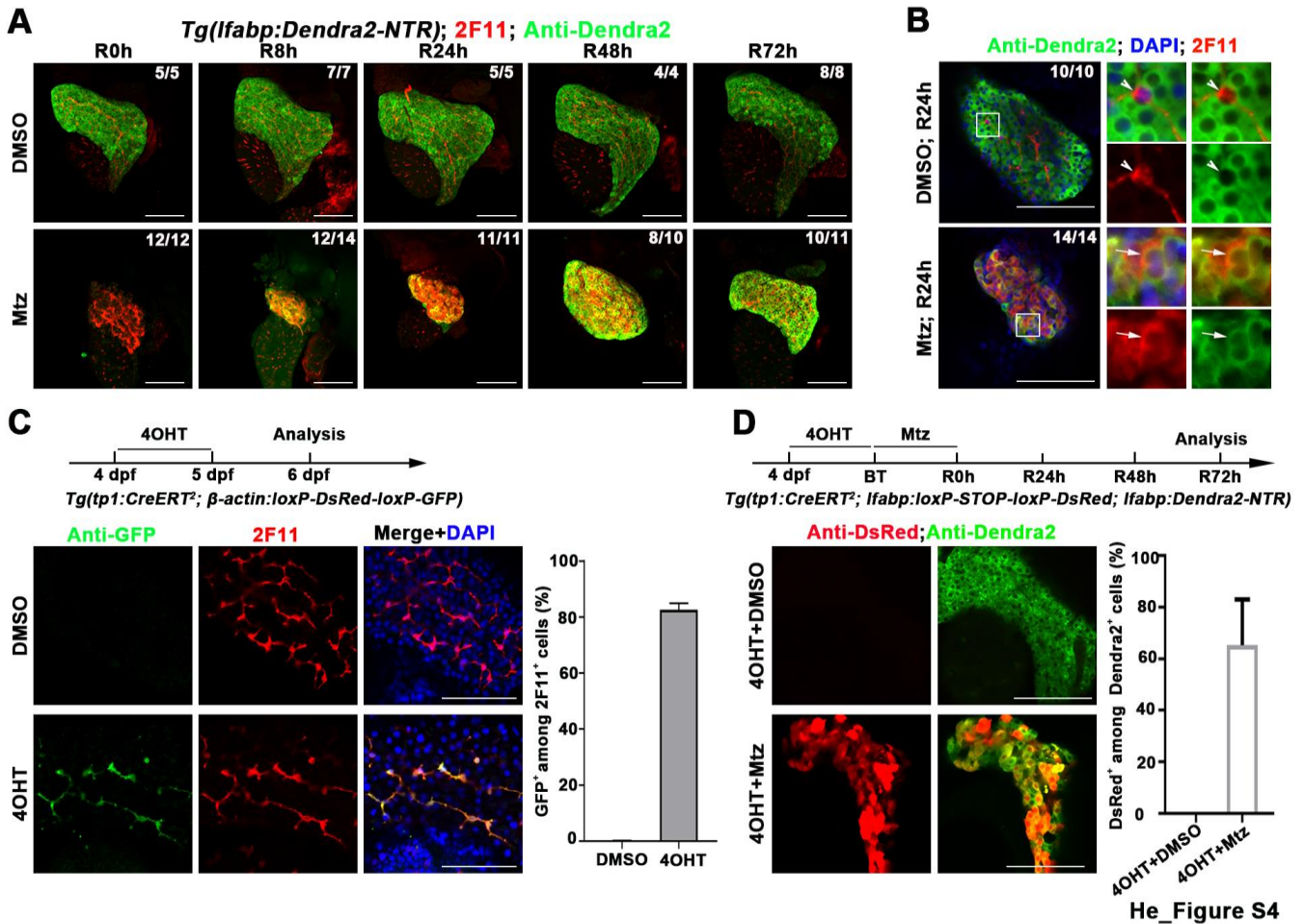
Figure S4. Lineage tracing of BECs during hepatocyte regeneration after extreme injury to healthy liver. Related to Figure 4. (**A**) Confocal projection images (3D imaging) showing the co-immunostaining for 2F11 and Dendra2 in liver regeneration after Mtz treatment. (**B**) Single-optical images showing the expression of 2F11 and Dendra2 at R24h in DMSO and Mtz treatment. There are no 2F11 and Dendra2 double-positive cells in DMSO treated liver (arrowheads); most of the new regenerating hepatocytes are 2F11 positive in Mtz treatment (arrows). Nuclei were stained with DAPI (blue). (**C**) Experimental scheme illustrating the stage of 4OHT treatment to double transgenic line, *Tg(tp1:CreERT2; β-actin:loxP-DsRed-loxP-GFP)* from 4 dpf to 5 dpf and analysis at 6 dpf. Immunostaining for 2F11 and GFP on livers (2D imaging) showing *tp1-CreER* labels the 2F11 positive cholangiocytes specifically after 4OHT treatment. Nuclei were stained with DAPI (blue). Quantification of the percentages of GFP+ among 2F11+ hepatocytes (DMSO, n=6; 4OHT, n=6). (**D**) Experimental scheme illustrating the stage of 4OHT and Mtz treatment and analysis at R72h. Single-optical images showing the expression of Dendra2 and DsRed in regenerating livers at R72h after 4OHT and Mtz treatment and control. Most of the new regenerating hepatocytes are DsRed positive. Quantification of the percentage of the DsRed+ among Dendra2+ cells (DMSO, n=10; 4OHT, n=10). Numbers indicate the proportion of larvae exhibiting the expression shown. Scale bars: 100 μm. Data are represented as mean ±SEM.
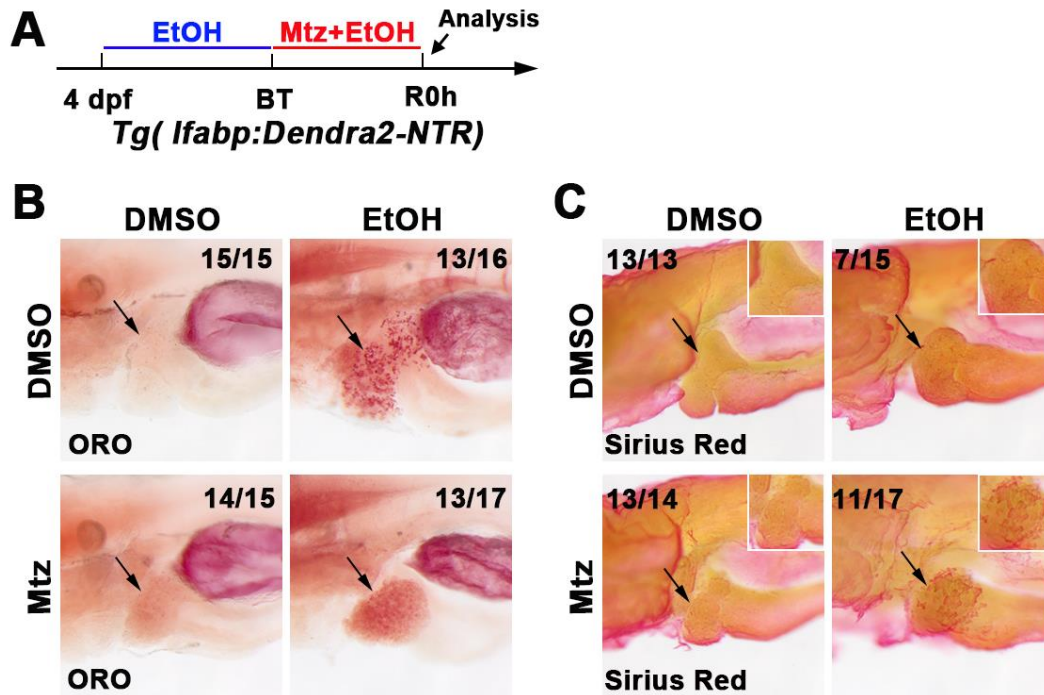
Figure S5. Establishing an Ethanol-induced Fibrotic Liver Model in Zebrafish. Related to Figure 4. (**A**) Experimental scheme illustrating the stage of EtOH and Mtz treatment in transgenic line *Tg(lfabp:Dendra2-NTR)*. (**B**) ORO staining shows fat deposits in livers after DMSO, EtOH, MTZ, and MTZ plus EtOH treatment at 6 dpf and R0h. The black arrowhead indicates the liver. (**C**) Sirius Red staining shows liver fibrosis after DMSO, EtOH, MTZ, and MTZ plus EtOH treatment at 6 dpf and R0h. The black arrowhead indicates the liver and the magnified liver regions were in a white box.

TRANSPARENT METHODS

CONTACT FOR REAGENT AND RESOURCE SHARING

Further information and requests for reagents may be directed to and will be fulfilled by the Lead Contact, Jianbo He (hejianbo@swu.edu.cn).

EXPERIMENTAL MODEL AND SUBJECT DETAILS

Animal Strains

The zebrafish facility and study were approved by the Institutional Review Board of Southwest University (Chongqing, China). Zebrafish were maintained in accordance with the Guidelines of Experimental Animal Welfare from Ministry of Science and Technology of People's Republic of China (2006) and the Institutional Animal Care and Use Committee protocols from Southwest University (2007). A complete list of the zebrafish strains is provided in the Key Resources Table. For the study both sexes were used.

METHOD DETAILS

Cell Sorting and Analysis

The *Tg(tp1:CreERT^2; lfabp:DenNTR; lfabp: loxP-STOP-loxP-DsRed)*, *Tg(krt18:CreERT^2; lfabp:DenNTR; lfabp:loxP-STOP-loxP-DsRed)*, and *Tg(lfabp:CreERT^2; lfabp:DenNTR; lfabp:loxP-STOP-loxP-DsRed)* transgenic larval and adult livers were dissected and dissociated in 0.5% Trypsin solution (0.5% trypsin and 1 mM EDTA in PBS, pH 8.0) for 5-10 minutes. Dissociated cells were collected by centrifugation at 3000×g for 2 minutes, resuspended in 1 ml PBS, and filtered using 40 μm cell strainers (Falcon). Then, cells were Analyzed using a Moflo XDP Fluorescence-Activated Cell Sorter (Beckman), Dendra2 and DsRed positive cells were analyzed.

Generation of Transgenic Lines

Lfabp-CreERT^2 construct was generated by replacing the *Dendra2-NTR* with *CreERT^2* in the *pBluescript2(+) lfabp:Dendra2-NTR* vector. For the generation of *Tg(lfabp:CreERT^2)* line, the construct *lfabp-CreERT^2* was digested with I-sce1 and injected into zebrafish embryos of AB background at the 1-cell stage. For the generation of *Tg(tp1:CreERT^2)* line, the construct *tp1-CreERT^2* (a gift from Michael Parsons) was co-injected with *tol2* mRNA into zebrafish embryos of AB (wide type) background at the 1-cell stage.

Antibody Staining and Imaging

The process was performed according to previously described (Chen et al., 2019; Lu et al., 2013). Briefly, larvae and adult liver were fixed with 2% formaldehyde in 0.1 M PIPES, 1 mM MgSO4, 2 mM EGTA, pH 7.0 at 4°C overnight. For the larval experiments, the skin was manually removed, and the larvae were washed three times with PBS. For the adult liver, the whole liver was embedded into 4% low-melting agarose, sectioned in 50 μm, and followed by incubation with acetone at -20°C for 30 minutes. After being washed three times with the washing solution (1% Triton X-100 in PBS) and blocked in the blocking solution (4% BSA, 0.02% NaN3, 1% Triton X-100 in PBS) for an hour at 4°C, larvae were incubated with antibodies against Dendra2 ((1:1000; AB821, Evrogen,

Moscow, Russia), GFP (1:1000; ab6658, Abcam, Cambridge, MA), 2F11 (1:1000; ab71826, Abcam, Cambridge, MA), Anti-Alcam (1:50; ZN-5, ZIRC), Anti-collagen 1 (1:100; ab23730, Abcam, Cambridge, MA) and DsRed2 (1:1000; sc-101526, Santa Cruz, Dallas, TX) diluted in the blocking solution at 4°C overnight. Then, larvae were washed five times with the washing solution for 40 minutes each and incubated with Alexa fluorescent-conjugated secondary antibodies (1:1000; Invitrogen, Grand Island, NY) diluted in the blocking solution at 4°C overnight. After washed five times with the washing solution, larvae were proceeded for mounting and imaging.

Whole-mount *in situ* hybridization

The process was performed according to previously described (Liu et al., 2016). Briefly, larvae were fixed with 4% paraformaldehyde (PFA) in PBS at 4°C overnight, followed by incubation in 100% methanol at -20°C for at least 24 hours. Larvae were serially transferred into 75%, 50%, 25%, and 0% methanol in PBT (0.1% Tween in PBS). Then the larvae were digested with Proteinase K (5 μg/ml in PBT, 1:2000 dilution) for 40min. Refixation in 4% PFA in PBS, 30 min at room temperature, the larvae were washed in PBT four times. Then the larvae pre-hybridized in HYB (50% formamide, 5×SSC, 0.1% Tween20, 5 mg/ml torula yeast RNA, 50 mg/ml heparin) at 65°C for 2 hours. Digoxigenin-labeled probes were then administrated, and hybridizations were carried out at 68.5°C overnight. After removal of probes, the larvae were serially washed at 65°C with 100%, 75%, 50%, 25% HYB in 2×SSCT, and finally with 0.2×SSCT. Afterwards, the larvae were serially incubated with 25%, 50%, 75% and 100% MABT (150 mM maleic acid, 100 mM NaCl, 0.1% Tween-20, pH 7.5) in 0.2×SSCT, then blocked for 2 hour with 2% Block Reagent (Roche, 11096176001) in MAB. Anti-Dig AP (Roche, 11093274910) were administrated at a 1:2000 dilution and incubated at 4°C overnight. The larvae were serially washed with MABT for eight times, After the larvae were washed with NTMT (100 mM Tris HCl pH 9.5, 50 mM MgCl$_2$, 100 mM NaCl, 0.1% Tween 20) for three times. During last wash, transfer embryos to a 24 well plate. Then incubated embryos in BCIP/ NBT staining solution (Roche, 11681451001, 1:50) at room temp or 4°C in the dark, without shaking.. Stop the reaction by removing the staining solution and washing the embryos 3x in PBT, then washed and stored in STOP solution (0.05M phosphate buffer pH 5.8, 1mM EDTA 0.1% Tween). The Whole-mount *in situ* hybridization (WISH) images were captured using the SteREO Discovery V20 microscope (Carl Zeiss, Germany). The template for *cp* antisense probes were amplified with the following primer, forward primer: 5'-CTGCGGAGGAGGACGACACGG-3', reverse primer: 5'-ATTGTAATACGACTCACTATAGGGGCATGTCGACACCGTCAGCC-3'. The template for *gc* antisense probes were amplified with the following primer, forward primer 5'-CCTCCAAGTCATTGGAATTG-3', reverse primer: 5'-ATTGTAATACGACTCACTATAGGGCGGAATGGGTACGACTGGAC -3'. Digoxigenin-labeled probes were generated by in vitro transcription (DIG RNA Labeling Kit, Roche).

Ethanol and Metronidazole Treatment

The *Tg(lfabp:Dendra2-NTR)^{cq1}* transgenic larvae at 5 dpf was incubated with 10 mM Mtz (Sigma-Aldrich) in 0.2% DMSO for 24 hours. Then, larvae were washed three times and recovered in egg water marking the 0 hour-post treatment (hpt) point. For ethanol (EtOH) treatment, the larvae were pretreated with 1.5% EtOH (vol/vol) (Sigma-Aldrich) from 4 dpf and from 5 to 6 dpf treated with 10 mM MTZ in 1.5% EtOH for 24 hours (Huang et al., 2014). After washing the MTZ, the larvae were incubated in 1.5% EtOH.

Temporal Control of CreERT^2 Activities

4-hydroxytamoxifen (4OHT; Sigma) was dissolved in 100% DMSO to prepare a stock concentration of 10 mM. Working concentrations were titrated, and 2-5 μM (pre-warm at 60°C for 20 minutes and shake at 37°C for 1 hour) was found to be optimal to induce the Cre-mediated recombination without leading to physiologically deleterious defects. For *Tg(tp1:CreERT^2; lfabp:DenNTR; lfabp: loxP-STOP-loxP-DsRed)*, larvae were incubated with 2 μM 4OHT in egg water at 28°C from 5 dpf to 7 dpf for 48 hours and 5 μM 4OHT in egg water at 28°C from 4 dpf to 5 dpf for 24 hours, respectively. For *Tg(tp1:CreERT^2; β-actin:loxP-DsRed-loxP-GFP)*, larvae were incubated with 2 μM 4OHT in egg water at 28°C from 5 dpf to 7 dpf for 48 hours, and 5 μM 4OHT in egg water at 28°C from 4 dpf to 5 dpf for 24 hours, respectively. For *Tg(tp1:CreERT^2; β-actin:loxP-DsRed-loxP-GFP)* and *Tg(tp1:CreERT^2; lfabp:DenNTR; lfabp: loxP-STOP-loxP-DsRed),* larvae were incubated with 5 μM 4OHT and 1.5% EtOH (vol/vol) in egg water at 28°C from 4 dpf to 5 dpf for 24 hours. For *Tg(krt18:CreERT^2; lfabp:DenNTR; lfabp:loxP-STOP-loxP-DsRed)* and *Tg(krt18:CreERT^2; β-actin:loxP-DsRed-loxP-GFP),* larvae were incubated with 2 μM 4OHT in egg water at 28°C from 10 dpf to 11 dpf for 24 hours. For *Tg(lfabp:CreERT^2; lfabp:DenNTR; lfabp:loxP-STOP-loxP-DsRed)* larvae were incubated with 2 μM 4OHT in egg water at 28°C from 5 dpf to 7 dpf for 48 hours. Then, larvae were washed three times and recovered in egg water.

Hematoxylin and Eosin Staining

For liver histology analysis, the embryos at 7 dpf were fixed in 4% PFA at 4°C overnight, serially dehydrated in ethanol, xylene and embedded in paraffin. The liver paraffin-sections (7 μm) were stained with hematoxylin and eosin according to the manufacturer's instruction.

Oil Red O Staining

Add 0.5 g Oil Red O (ORO) (BBI Life Sciences) to 100 ml 100% isopropyl alcohol as ORO stock solution. Larvae were fixed with 4% PFA at 4°C overnight. The larvae were washed with PBS, then washed with 60% isopropanol for 1 hour, stained with filtered ORO working solution (3 part ORO stock solution to 2 part H_2O) (for 15 min at room temperature, and then washed twice with H_2O for 15 min.

Sirius Red Staining

Larvae were fixed with 4% PFA at 4°C overnight. The larvae were washed with PBS, removed the skins, then stained with 10% Sirius Red staining solution (SenBeiJia Life Sciences) for 10min at room temperature. Then washed twice with H_2O for 15 min.

Partial Hepatectomy of Zebrafish larvae

Larvae from 5 dpf were embedded in 1% low melting agarose (Life Science), and the liver was dissected and resected with sharp tweezers (55#, WPI) under the fluorescent microscope at 50 x amplification. After PH, the larvae were bred in the egg water at 28.5°C.

Quantification and Statistical Analysis

zebrafish were imaged using a SteREO Discovery V2.0 microscope equipped with AxioVision Rel 4.8.2 software (Carl Zeiss). Antibody stained and imaged using ZEN 2010 software equipped on an LSM780 and LSM880 confocal microscope (Carl Zeiss). All figures, labels, arrows, scale bars, and outlines were drawn using the Adobe Photoshop software. Unpaired two-tailed Student's t-test was used for statistical analysis; P<0.05 was considered

statistically significant. Quantitative data were shown as means ±SEM. The exact sample number (n), *P* value for each experimental group and statistical tests were indicated in the figure legends.

SUPPLEMENTAL TABLE S1–KEY RESOURCES

REAGENT or RESOURCE	SOURCE	IDENTIFIER
Antibodies		
Rabbit anti-Dendra2 (1:1000)	Evrogen	Cat# AB821
Rabbit anti-Collagen 1 (1:100)	Abcam	Cat#ab23730
Mouse anti-Alcam (1:50)	Zebrafish International Resource Center	Cat# zn-5
Goat anti-GFP (1:1000)	Abcam	Cat#ab6658
Mouse 2F11 (1:1000)	Abcam	Cat#ab71826
Mouse anti-DsRed (1:1000)	Santa Cruz	Cat#SC-101526
Donkey anti-goat IgG Alexa fluor 488-conjugated (1:1000)	Invitrogen	Cat#A11055
Donkey anti-goat IgG Alexa fluor 633-conjugated (1:1000)	Invitrogen	Cat#A11057
Donkey anti-mouse IgG Alexa fluor 568-conjugated (1:1000)	Invitrogen	Cat#A10073
Donkey anti-mouse IgG Alexa fluor 647-conjugated (1:1000)	Invitrogen	Cat#A31571
Donkey anti-rabbit IgG Alexa fluor 488-conjugated (1:1000)	Invitrogen	Cat#A10042
Anti-Dig-AP (1:2000)	Roche	Cat#11093274910
Chemicals, Peptides, and Recombinant Proteins		
NBT/BCIP Stock Solution	Roche	11681451001
Ethanol (EtOH)	Sigma-Aldrich	P7023
Low-melting agarose	BBI Life Sciences	A600015-0025
4-Hydroxytamoxifen (4OHT)	Sigma-Aldrich	H7904
Metronidazole (Mtz)	Sigma-Aldrich	M3761
Oil Red O	BBI Life Sciences	A600395-0050
Critical Commercial Assays		
Sirius Red staining solution	SenBeiJia Life Sciences	BP-DL030
Hematoxylin staining solution	BBI Life Sciences	E607317-0100
Eosin staining solution	BBI Life Sciences	E607321-0100
Experimental Models: Organisms/Strains		
Zebrafish: *Tg(lfabp:DenNTR)*[cq1]	He et al., 2014	ZFIN:ZDB-ALT-150922-3
Zebrafish: *Tg(krt18:CreERT2)*[cq74]	He et al., 2019	N/A

Zebrafish: *Tg(lfabp:loxP-STOP-loxP-DsRed2)^{cq4}*	He et al., 2014	ZFIN:ZDB-TGCONSTRCT-150922-5
Zebrafish: *Tg(tp1:CreERT^2)*	This study	N/A
Zebrafish: *Tg(lfabp:CreERT^2)*	This study	N/A
Recombinant DNA		
pBluescript-lfabp-CreERT^2	This study	N/A
Tol2-tp1-CreERT^2	Wang et al., 2011	N/A
Software and Algorithms		
ZEN2010 Imaging software	Carl Zeiss	https://www.zeiss.com
AxioVision Rel 4.8.2 software	Carl Zeiss	https://www.zeiss.com
GraphPad Prism	GraphPad	https://www.graphpad.com
Moflo XDP Fluorescence-Activated Cell Sorter	Beckman	https://www.beckmancoulter.com

SUPPLEMENTAL REFERENCES

Chen, J., He, J., Ni, R., Yang, Q., Zhang, Y., and Luo, L. (2019). Cerebrovascular Injuries Induce Lymphatic Invasion into Brain Parenchyma to Guide Vascular Regeneration in Zebrafish. Developmental Cell *49*, 697-710.

Liu, C., Wu, C., Yang, Q., Gao, J., Li, L., Yang, D., and Luo, L. (2016). Macrophages Mediate the Repair of Brain Vascular Rupture through Direct Physical Adhesion and Mechanical Traction. Immunity *44*, 1162-1176.

Lu, H., Ma, J., Yang, Y., Shi, W., and Luo, L. (2013). EpCAM is an endoderm-specific Wnt derepressor that licenses hepatic development. Dev Cell *24*, 543-553.